(2)

FINAL TECHNICAL REPORT

INVESTIGATION OF UNDERWATER OBJECTS SEPARATION

IN A CROSS-FLOW

Contract N00167-88-K-0058

Submitted by

Prof. Karol Z. Korczak, P.I.
Mechanical and Aerospace Engineering
Case Western Reserve University
10900 Euclid Avenue, Cleveland, Ohio 44106

ONR Program Manager - James A. Fein
Contract Scientific Officer - V.J. Monacella

ABSTRACT

The research project has been initiated to develop a numerical algorithm and conduct a broad investigation of flow structures and their interactions with moving and ejecting objects. The numerical method is based on a spectral element approach applied to the unsteady, incompressible Navier-Stokes equations. The equations are adopted for a moving mesh system that allows the mesh to adjust dynamically to changing geometry. The method has been used to study flow patterns and forces on moving objects. Among the investigated cases are: two- and three-dimensional piston pumps, flow through an oscillating channel, an oscillating cylinder in a still fluid, an oscillating cylinder in a uniform flow, and an ejecting object from a silo.

PROJECT SUPPORT

The project has been supported by the Office of Naval Research, Applied Hydrodynamics Research Program. The support continued for the period April 28, 1988 to July 15, 1990. The research continued without funding until March 30, 1991.

The project supported a graduate student, Mr. Robert A. Jusups, working for an M.S. degree which he received in August 1990.

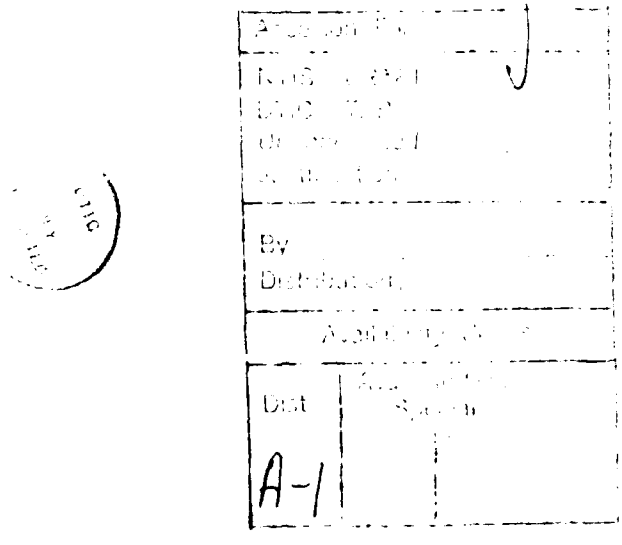

INTRODUCTION

Real flow cases with objects deforming or moving within the flow are quite common. Machines with moving parts, structures deforming or vibrating in the wind or water current, artificial heart pumping blood, opening and closing valves, aircraft dropping bombs, submarines ejecting torpedoes or launching missiles. These examples represent but few. Numerical simulations of such cases are not common due to relatively high complexity of the geometry involved, numerical difficulties with handling nonstationary meshes, high complexity of the unsteady flow fields, and large CPU demands. Even experimental investigations are relatively rare and the evidence in literature is even more limited due to the fact that some of the research involved classified data or results. In many cases, the scientific rewards for the unavoidable significant research effort might not be as attractive as in more traditional areas.

In this study, the primary focus was on phenomena associated with ejection of objects into surrounding fluid. However, several other cases were investigated for comparison of numerical and experimental results and to determine overall possibility of such investigations.

The spectral element method [1-9] was adopted for this investigation. The method was reformulated to allow the deformations and motion of the numerical mesh which followed the moving objects. Initially, a piston pump was simulated (two- and three-dimensional) to provide a test case for the method and to allow qualitative comparisons with existing experimental evidence [10,11].

The problems of underwater motion, ejection, and separation has been the focus of several investigations [12-20], primarily associated with military applications such as launches from submarines of missiles or torpedoes. More general applications are associated with oscillating slim underwater structures [21-29] such as cylindrical supports of oil platforms and bridges. That category includes also toll buildings and chimneys subjected to the forces resulting from air flow.

This investigation simulated and analyzed many of those type of flows with results described in the following sections. The analysis in most cases could not be extensive due to the very large CPU time needed to advance the simulation. Unfortunately, this is the primary limiting factor in advancing the numerical analysis for cases like the ones mentioned above beyond research interest to result in a design tool.

NUMERICAL APPROACH

The numerical method implemented for this project is based on the spectral element method which is a blend of a spectral approach [1,2,3] and finite element technique. The spectral element technique underwent many modifications from its initial formulation [4,5] to expand the realm of applications. The approach resembles the h-version of finite elements [6]; however, due to spectral local expansions, it is much more accurate and suitable for complex flow simulations [7-8].

As in finite elements, the approach breaks the domain into a series of subdomains mapped from the physical space (x,y,z) into local space (r,s,t) where they are a regular cubes ranging from -1 to +1 along each axis. The geometry, velocity, and pressure are represented as tensor-product high order Lagrangian interpolants (based on Legendre polynomials) through Gauss-Lobatto points. Those points are the roots of the first derivative of the Legendre polynomials and the end points. The equations are formed for each subdomain (element) and then combined into a global matrix system using the direct stiffness method (as in finite elements).

The approach uses the unsteady, incompressible Navier-Stokes equations [9] which together with mass conservation have the following form:

$$\frac{\partial v_i}{\partial t} + v_j \frac{\partial v_i}{\partial x_j} = -\frac{\partial}{\partial x_i}\left(\frac{p}{\rho}\right) + \nu \frac{\partial^2 v_i}{\partial x_j^2} + F_i \qquad (1.1)$$

and

$$\nabla \bullet V = 0 \qquad (1.2)$$

where:

$V = v_1\hat{i} + v_2\hat{j} + v_3\hat{k}$ = velocity
p = static pressure
ρ = density
ν = kinematic viscosity
F_i = body force

To solve the system, a splitting scheme is implemented with the following steps:

- nonlinear step:

$$\frac{(\tilde{v}_i^{n+1} - v_i^n)}{\Delta t} = -v_j \frac{\partial v_i}{\partial x_j} + F_i \tag{1.3}$$

- pressure step:

$$\frac{(\bar{v}_i^{n+1} - \tilde{v}_i^{n+1})}{\Delta t} = \frac{\partial}{\partial x_i}\left(\frac{p}{\rho}\right) \tag{1.4}$$

- viscous step:

$$\frac{(v_i^{n+1} - \bar{v}_i^{n+1})}{\Delta t} = \nu \frac{\partial^2 v_i}{\partial x_j^2} \tag{1.5}$$

The non-linear step is solved explicitly using the third-order Adams-Bashforth approach (no boundary conditions are needed here):

$$\frac{(\tilde{v}_i^{n+1} - v_i^n)}{\Delta t} = C_0\left(-v_j \frac{\partial v_i}{\partial x_j} + F_i\right)^n + C_1\left(-v_j \frac{\partial v_i}{\partial x_j} + F_i\right)^{n-1} + C_2\left(-v_j \frac{\partial v_i}{\partial x_j} + F_i\right)^{n-2} \tag{1.6}$$

where $C_0 = 23/32$, $C_1 = -16/12$, $C_2 = 5/12$.

The system above performs satisfactorily if the Courant number ($\frac{v\Delta t}{\Delta x}$) is not greater than 0.5. The pressure step is solved implicitly. The known pressure is imposed at input as Dirichlet boundary condition with natural boundary conditions everywhere else. The viscous step is solved using

Crank-Nicholson approach with the required boundary conditions on velocity. At the outflow, the natural boundary conditions are imposed.

To allow dynamic changes of the mesh during simulations, the momentum equations must be modified to account for that additional motion. To achieve that, the new positions of the deforming mesh (moving mesh points) must be known. Together with the previous positions, the information is sufficient to find the new velocity and pressure fields at mesh points in the new locations. The reformulation of the momentum equation is fairly straightforward and does not add significantly to the complexity of the regular spectral element codes.

Let $\hat{x} = f(\hat{x}, t)$ to be the old position of the mesh and $x = f(x, t)$ to be the new position of the mesh. The old nodal velocity would then be $\hat{v} = \hat{v}(\hat{x}, t)$ and the new nodal velocity would then be $v = v(x, t)$. With these, the momentum equation at the new position with respect to the old position is given as:

$$\frac{\partial v_i}{\partial t} + \left(\frac{\partial x_j}{\partial t} + \frac{\partial x_j}{\partial \hat{x}_j} \times v_j\right)\frac{\partial v_i}{\partial x_j} = \frac{\partial x_j}{\partial \hat{x}_j}\frac{\partial}{\partial x_i}\left(\frac{p}{\rho}\right) + \left(\frac{\partial x_j}{\partial \hat{x}_j}\right)^2 \nu \frac{\partial^2 v_i}{\partial x_j^2} + F_i \qquad (1.8)$$

Let $\alpha_j = \frac{\partial x_j}{\partial t}$ be the velocity of the mesh nodes and $\beta_j = \frac{\partial x_j}{\partial \hat{x}_j}$ be the local deformation of the mesh. Withe these, the final form of the momentum equations is as follows:

$$\frac{\partial v_i}{\partial t} + (\alpha_j + \beta_j v_j)\frac{\partial v_i}{\partial x_j} = -\beta_i \frac{\partial}{\partial x_i}\left(\frac{p}{\rho}\right) + \beta_j^2 \nu \frac{\partial^2 v_i}{\partial x_j^2} + F_i \qquad (1.9)$$

During flow simulation, the new position of the mesh is determined, the above coefficients are calculated and the new flow field is computed. The extra work associated with the moving mesh is relatively small, probably no more than 5% in CPU time. The benefit of this approach is that no additional approximations are necessary and that the flow field "follows" the mesh.

One must be careful not to allow the mesh to deform too much. If the deformations are too excessive, the errors due to those deformation might cause serious problems for accuracy and most of all for convergence of iterative solvers.

NUMERICAL SIMULATIONS

The study involved several cases of flows associated with moving geometries. Most of the cases were investigated to determine the method's performance and ability to handle such flows. The numerical results were compared when possible with existing experimental evidence. Both two- and three-dimensional cases were considered.

Two-Dimensional Piston Pump

The two-dimensional piston pump (Figure 1) has a mesh with 26 spectral elements, 25 of them constitute the inside of the cylinder and the 26th element resides in the inflow neck. Each element has 125 nodes; the top and the bottom of the geometry are curvilinear to resemble an actual pump.

During a pumping cycle, the volume increases 2.6 times with respect to the initial volume. The numerical conditions on pressure impose a fixed pressure at inflow; therefore, an area around the center of the piston surface has been designated as "numerical" inflow with velocity equal to the velocity of the piston itself. This arrangement fixes an area with the reference pressure (here set to zero for convenience) and preventing any flow through the piston surface. The flow may enter or exit only through the inflow neck.

The motion of the piston is enforced to follow a cosine curve. The peaks of the piston's displacement correspond to zero velocity. The maximum velocity occurs in the midpoint of the piston cycle. One piston cycle takes 1500 time steps which corresponds to 46.75 time units for the code. In SUN 3/50 CPU time, it requires 84 hours to run a full cycle. The velocities on the moving piston surface are calculated every step and imposed appropriately for the flow calculations.

As expected, the rapid expansions and contractions of the pump volume are creating complex vortex structures (Figure 2). To avoid the influence of the initial conditions, the results are recorded starting with the third cycle of the simulations.

Three-Dimensional Piston Pump

The mesh for the pump contains 57 spectral elements (Figure 3) with 125 nodes each. As in the two-dimensional case, the mesh has four layers of elements with thirteen elements per layer. The surface of the piston and the head of the cylinder chamber are curvilinear. The inlet has five elements in it. The pump's volume expands twice with respect to its initial state. The piston motion follows a cosine curve. One full cycle requires 1700 time steps which corresponds to 49.61 time

units. In SUN 4/110 CPU time units, it takes 600 hours per cycle. Due to the excessive simulation time, the experiment was curried only through one and a half cycle.

The flow field is documented in Figure 4. Due to the acceleration and deceleration of the piston, the flow patterns exhibit complex vortex structures forming in the cylinder chamber.

The results of this simulation have been compared qualitatively with the experimental results obtained by Durst, Ernst, and Pareira [10] using laser doppler anemometer. The experimental results were processed numerically for visualization [11] and are almost identical to those shown in Figure 5.

The 3-D numerical simulation exhibits all the details of the flow demonstrated in the experimental investigation. The 2-D simulations show more extensive vortex structure field due to the constraint coming from the two-dimensionality.

The Oscillating Channel

The dynamic motion of geometries in a flow results in variable forces and moments acting on those objects. Those forces and moments were recorded in the simulation of a flow in a three-dimensional, rectangular, oscillating channel (Figure 6).

The channel consists of six elements with 343 nodes per element. The motion imposed on the channel is a sinusoidal oscillation of the exit section with an amplitude of one-fifth the channel height in a direction perpendicular to the flow. Forces are recorded on the upper and lower walls. The moment is calculated at a point which acts as a hinge for the oscillation located at the center of the bottom wall in the spanwise direction. With a time step of 0.0424, forces and moments are recorded every three time steps. A full cycle consists of 300 time steps which corresponds to nine CPU hours of SUN 3/50.

As the channel oscillates, the motion of the walls imposes a velocity on fluid near the wall (Figure 7). During the oscillation, the inertia of the fluid causes pockets of high pressure to appear near the inlet and pockets of low pressure to occur near the outflow. As expected, moments and forces display sinusoidal oscillations synchronized with the geometrical motion (Figure 8).

The results from this simulation allow a qualitative evaluation of the method's capability to determine forces and moments resulting from geometry-flow structures interactions. For quantitative evaluations (calibration) more extensive simulations and actual experimental measurements would have to be conducted.

Analysis of Cylinders Oscillating in a Still Fluid and in a Uniform Flow

Introduction

Analysis of the flow around an oscillating cylinder in a still fluid and in a uniform flow shows that these cases are quite different than flow in the classical case of a cylinder in a steady, uniform flow. An oscillating cylinder reverses direction, causing the vortex wake of one half cycle to sweep past the cylinder during a subsequent half cycle. This reversal has a major effect on the magnitudes of fluid induced forces and also on the fundamental frequency of the drag force.

The interest in studying flow around oscillating cylinders has arisen from many modern day construction problems. Vortex induced vibrations are often the cause of costly construction delays and failures in offshore structures such as underwater piping and cylindrical structure components. Civil engineers have encountered similar problems with cylindrical columnar buildings and chimney stacks in a crosswind. Force oscillations are a significant factor when considering the fatigue life of a structure. Furthermore, there is a considerable fundamental interest in these flows and in the ways in which vortices are generated and shed.

For years, designers of offshore platforms typically have used what is known as the Morrison force equation [21] to calculate the wave on offshore cylindrical structures. The Morrison description considers the force to be composed of a drag force (described by the standard semi-empirical drag coefficient relation) and an inertia force (described in terms of the inertial coefficient which is related to the hydrodynamic added mass coefficient) [22].

For a circular cylinder, the in line force per unit length is:

$$F = \frac{1}{2}\rho D C_d U|U| + \frac{1}{4}\pi\rho D^2 C_m \frac{dU}{dt}$$

where: ρ - fluid density
D - body diameter
U - fluid velocity
C_m - coefficient of mass
C_d - coefficient of drag

The coefficients C_m and C_d have been evaluated experimentally from full-scale and laboratory studies by a considerable number of investigators. This is usually done with the method of least squares or using the Fourier averaging over a cylinder cycle [23].

Keulegan and Carpenter [24] have found that the average values of C_m and C_d are functions of

the oscillating cylinder's amplitude and diameter. When the relative flow past a cylinder is undergoing sinusoidal oscillations, the Keulegan-Carpenter number KC is defined as $(2\pi a)/d$; where a is the amplitude of the relative motion and d is the cylinder diameter. Sarpkaya [23] has found that C_m and C_d depend not only on KC, but also on a parameter β which is proportional to the Reynolds number Re: $\beta = (Re)/(KC) = D^2/Tv$, where T is the period of oscillation and v is the kinematic viscosity. This number is also known as the Stokes number, named after Stokes who in 1851 have shown that the force acting on a cylinder or a sphere oscillating sinusoidally in a viscous fluid is dependent on both the amplitude of the oscillations and the Reynolds number.

Williamson [25] has performed investigations on the relation between motions of vortices and forces exerted on a circular cylinder for various KC numbers. He did not examine the three-dimensional structure of the flow along the cylinder axis. Tatsumo and Bearman [26] examined this three-dimensional structure and concluded that at low KC numbers and at low Stokes numbers the flow around cylinders is two-dimensional. For this reason, a two-dimensional numerical simulations has a legitimate justification.

Numerical simulations have been used quite frequently to calculate flow around cylinders. Most of the time, the cylinders have been stationary due to difficulties associated with the moving geometry. The major problem has been with describing boundary conditions at the continuously accelerating or decelerating solid wall using the finite element or finite difference traditional grid system [27]. The problem has been dealt with in different ways by many investigators [27,28].

The Two-Dimensional Oscillating Cylinder

As indicated above, a two-dimensional flow exists for small KC numbers. Furthermore, two-dimensional simulations can be conducted within a reasonable computer time, making this a useful tool for method verifications and preliminary studies.

In the case of this study, the two-dimensional cylinder mesh contains 40 spectral elements with 125 nodes per element (Figure 9). The cylinder has a unit radius and the mesh extends radially away from the cylinder to a distance of eight. This geometric domain has been deemed large enough by using experimental visualization results. All secondary and primary flow patterns produced by the oscillating cylinder will occur within this distance. Primary flows are defined as those which occur outside of the cylinder's boundary layer. Secondary flows are those which occur inside the cylinder's boundary layer.

A coordinate system has its origin in the center of the cylinder at initial position. The cylinder oscillates along the y-axis. Boundaries parallel to the y-axis are defined as inflows and the bound-

aries parallel to the x-axis are prescribed as outflows. Pressure as well as velocity are set to be zero at inflows.

Three test cases have been chosen, each with a different amplitude: 0.8*radius, 1.0*radius, 2.0*radius. According to the findings of Sorokodum [29], these three cases will result in three different flow fields. Parameters for the test cases are summarized in the table below:

	Test #1	Test #2	Test #3
Amplitude	0.8*radius	1.0*radius	2.0*radius
KC Number	2.5	3.2	6.3
Stokes #	62.7	30.8	30.8
Reynolds #	157.6	96.8	193.5

In all three cases the period of oscillations is 300 time steps. A sinusoidal motion is imposed for the cylinder. To avoid picking up flow patterns due to the start up of motion, results are recorded with the beginning of the second oscillation cycle. In SUN 3/50 CPU time, these computations averaged 168 hours.

The results of the simulations are presented on Figures 10, 11, 12, and 13. The results are in qualitative agreement with the works of Williamson, Tatsumo and Bearman, and Sarapkaya.

The Three-Dimensional Oscillating Cylinder

The three-dimensional cylinder mesh contains 100 spectral elements with 125 nodes per element (Figure 14). The mesh is an extension of the two-dimensional case in the third dimension. The cylinder is set to oscillate with an amplitude equal to its radius and period of oscillations equal to 3.1 time units (300 time steps).

The three-dimensional case, due to extensive requirements for CPU time, has been curried only for a limited time to determine dynamic forces acting on the cylinder. Two runs were performed at a free stream Reynolds number of 80 and 120, and a KC number of 3.14. Forces on the entire cylinder were recorded every two time steps. The moment of forces is calculated with respect to the center of the cylinder. The results are shown on Figure 15.

The results conform to experimental results. The forces are plotted as a function of time and as a function of velocity. The relation between forces and velocities in that type of motion was used by Hamann and Dalto [22] to try to find a nondimensional parameter to correlate forces due to wave action. Their findings show that the measured forces are more dependent on the velocity than

on the acceleration. They concluded that for a constant value of A/d the maximum force per unit area is a function of the actual velocity and that the force is increasing with the increase of the A/d ratio. The slope of the curve from the results of the current investigation is in agreement with those from experiments.

The Separating Object Case

Introduction

An initial objective to study full separation process of an object ejected into a flow field has been modified following suggestions from the David Taylor Research Center and focussed on the interactions during the initial stages of an object plowing into bay and then into the surrounding flow field. The geometry adopted for this investigation is shown below.

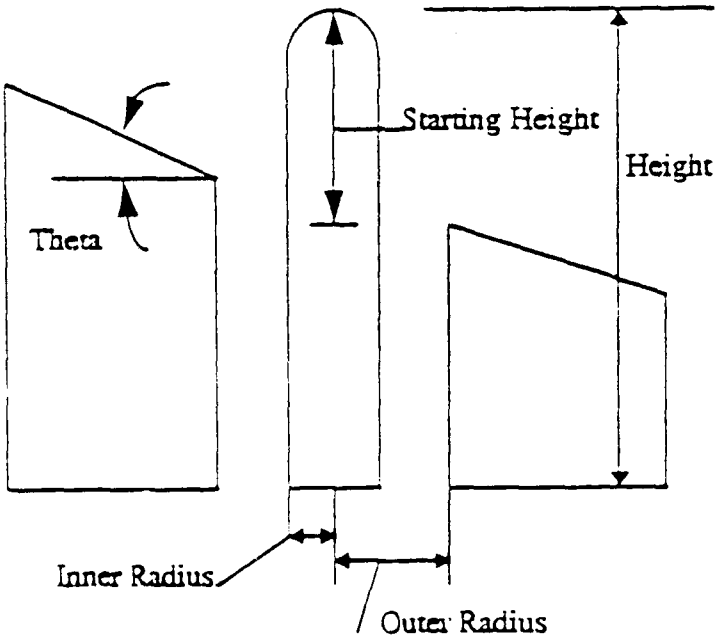

There is a scarce information in literature on this subject. Most of the work done has been experimental and theoretical and was directed towards underwater bodies. The available papers present an evidence that can be divided into four groups of interests: a) equations of motion of sub-

merged bodies [14,15], b) water entry and exit problems [16,17], c) forces acting on submerged bodies [18,19] and d) journal articles related to missiles and submarines [13,20]. Most of the research is considered classified and, therefore, with limited access.

The case under investigation in this research involves the geometry configuration shown earlier. The object, initially in the silo, is pushed into the surrounding fluid until the moment when separation would occur. The interest here is on the flow structures, forces, and moments acting on the object during that initial stage of ejection. The ejection could be into a still fluid or into a cross-flow.

Due to a relatively complex geometry, an automated mesh generator routine has been created with five main parameters: the object (inner) radius, the silo (outer) radius, the angle of the silo's surface (theta), the height of the object, and the initial height of the object in the silo. The generated mesh consists of 193 spectral elements (Figure 16). The mesh is constructed in such a way that when all elements are in their unstretched configuration, the object is fifty six percent of its lengths above the silo. In that position, the object's length to diameter ratio is 5.5:1 which resembles the proportions for a Trident C4 missile.

The way the mesh changes during the ejection process affects the accuracy and speed of the calculations due to the fact that matrix solvers are based on iterative schemes and more distorted elements require more iterations to converge to a solution. In addition, it was discovered that there might be a considerable difficulty to impose properly the conditions for non-zero velocity on the outside flow if the surface of the mesh is complicated.

The object is assumed to be pushed out of the silo with the necessary force. At the same time, the fluid will be pushed through the annulus into the surrounding flow field. The flow of that fluid is prescribed by the following relation (for a flow through a concentric annulus with a moving inner wall):

$$V_a = (r^2 - a^2) - \left(\frac{((a^2 - b^2) + V_{wall})}{ln(\frac{b}{a})} \right) \times ln(\frac{r}{a})$$

$$V_r = 0$$

where
a - radius of the object
b - radius of the silo
V_{wall} - object's velocity
V_a - axial velocity component
V_r - radial velocity component

Stationary Object Case

The first investigated case was set with the following parameters: object radius=0.6, silo radius=1.2, object height=6.6, object height above silo=3.76, theta=60 degrees. The object was kept stationary and the flow in the annulus was initiated with maximum velocity at the inlet to the annulus being ramped from zero to its normal value (0.5 for this configuration) over 50 time steps. The ramping follows a cosine curve for smooth acceleration and deceleration of the entering flow. In addition, the flow was allowed to settle from the impact of the ramping for the next 50 time steps. The data for analysis was taken after 100 time steps of the numerical simulation. Figure 17 shows the flow and pressure fields which are as one might expect.

This case showed the main problem for simulations of that type: the overwhelming requirement for CPU time. On SUN 4/110 the first 100 time steps of the simulation took 432 CPU hours. With increasing complexity (more deformed mesh, more resolution), the required time grows quite dramatically. For that reason, it is very difficult to achieve developed states for the flow and pressure fields.

The simulation was repeated for similar parameters with theta=0 (flat silo surface). The results are shown in Figure 18. The velocity and the pressure are as expected in such cases. This case was used as a starting point (initial conditions) for the case with moving object.

Object Ejecting into Still Flow Field - Forced Motion

To allow the object to move in all directions, the elements in the mesh must be able to deform accordingly. In this particular case, the generated mesh contains two rings of elements (Figure 19) that change their shape to allow the object to move. When the object moves in the z-direction, elements in the innermost ring shrink or expand in the z-direction. Elements in the outermost ring then contract or expand in order that their innermost element faces match with the corresponding elements in the inner ring (Figures below).

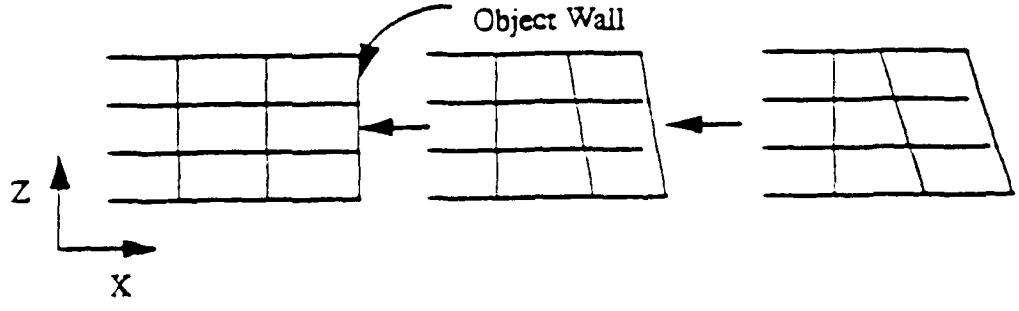

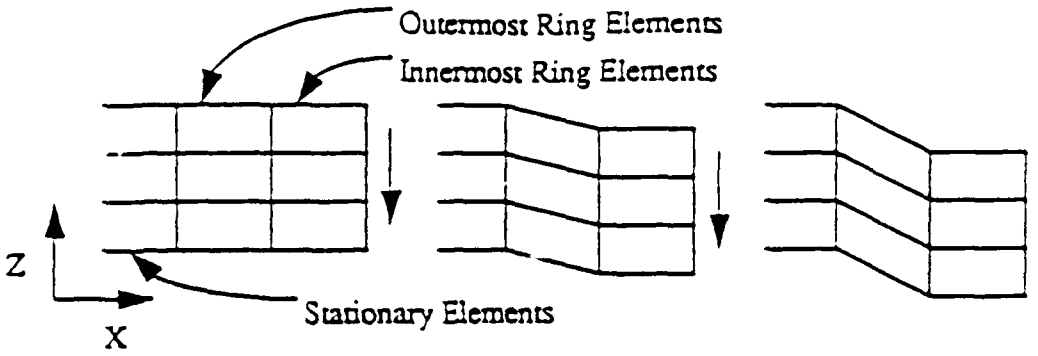

It is assumed in this case that the object can pivot with respect to the bottom of the silo (the inlet to the annulus). If the object moves in direction perpendicular to main motion, the mesh transforms accordingly to accommodate the new position. Rotation of the object with respect to its own axis does not cause any mesh deformations.

Several cases have been simulated with the object moving in and out of the silo. That motion generates intensive vortex structures in the vicinity of the object's tip. The addition of forced motion into x-y-directions creates quite complex flow fields (Figure 20) due to the fact that the object pushes and drags a large volume of fluid during side motions.

Object Ejecting into Cross-Flow - Forced Motion

Due to the complexity of the mesh changes during an object ejection cycle, the imposition of a cross-flow through proper boundary conditions above the surface of the silo exhibited some difficulties. In the current case, the top of the computational domain has been assigned an impermeable wall condition to force the flow to go along the surface of the silo. The velocity profile perpendicular to the silo surface was assumed to be Blasius profile for a boundary layer flow.

When the top of the computational mesh has fragmented boundary conditions (part with Dirichlet type, part with Neuman type), the junctions of the various types of the boundary conditions did not functioned properly creating corner type flows and other problems. The mesh should be constructed in a way that will assure uniform boundary conditions on the top section of the mesh where the surrounding fluid interacts with the flow patterns generated by the ejecting body.

The simulation was initially done for immobilized object followed by object ejection cycle. The flow and pressure patterns (Figure 21) are complex in these cases and the simulations must be curried on for some time to diminish the influence of initial conditions. Unfortunately, the simulations are very CPU demanding which prevented the current investigation from getting fully developed flows and conducting more detailed study.

CONCLUSIONS

The results of the simulations indicate that the numerical flow analysis for such cases can be accurate and predict important flow phenomena. For three-dimensional cases combined with motion of bodies, the formulation becomes quite complex and requires significant resolution (large number of computational points). When the motion is significant, the mesh can become quite distorted and affect the accuracy and the speed with which a solution at a given time step is achieved, particularly with respect to a pressure step. A care must be taken to prevent excessive distortions of elements in meshes. With these aspects in mind, the numerical simulations serve as a very useful tool in research and practice involving cases as investigated in this project. The comparison between the simulations and the (when available) experimental data showed good qualitative agreement.

All simulations in the cases above were for situations in which the motions were forced on the moving objects and the resulting forces and moments from the body-fluid interactions calculated. However, knowing the forces and the moments (torques) acting on a moving body, it is fairly straightforward to develop a dynamic equations of motion for that body allows to determine the trajectory (path). That is essential for unconstrained bodies such as ejected objects. A preliminary program was developed for that purpose and initially tested. Due to the limited data from ejecting object simulations and time constraints, the dynamic motion solver has not been completed.

The main factor limiting the scope of this research was the large demand for CPU time, particularly for three-dimensional cases involving significant object motions (mesh distortions). The use of supercomputers, vector processors, and multiprocessor machines could improve that situations.

RECOMMENDATIONS FOR FUTURE RESEARCH

There is a significant interest on part of the industry for simulations involving moving objects and particularly for cases that require the simulation not only of the flow field but also the dynamic behavior of the body resulting from the external fluid forces. However, at present it seams that for realistic and accurate simulations of such cases, the required size of the computational model results in very large computing times. In addition, cases with large Reynolds numbers and highly unsteady further complicate the situation. Therefore, with the current computational capabilities (primarily supercomputers or comparable machines) one can approach only limited cases. Eventually, when the barriers of computer speed will be overcome by technological developments and new solvers for matrix equations (the main CPU time consumers) will be developed, the successful research developments in this area will offer scientific rewards as well as technological payoffs.

REFERENCES

[1] Gottlieb, D.O. and Orszag, S.A., Numerical Analysis of Spectral Methods: Theory and Applications, SIAM, Philadelphia (1977)

[2] Hussaini, M.Y. and Zang, T.A., "Spectral Methods in Fluid Dynamics," Annual Review of Fluid Mechanics, vol. 19, pp.339-367 (1987)

[3] Orszag, S.A., "Spectral Methods for Problems in Complex Geometries," Journal of Computational Physics, vol. 37, p.70 (1980)

[4] Patera, A.T., "A Spectral Element Method for Fluid Dynamics: Laminar Flow in a Channel Expansion," Journal of Computational Physics, vol. 54, p. 468 (1984)

[5] Korczak, Karol Z. and Patera, Anthony T., "An Isoparametric Spectral Element Method for Solution of the Navier Stokes Equations in Complex Geometry," Journal of Computational Physics, vol. 62, pp. 361-382 (1986)

[6] Babuska, I. and Dorr, M.R., "Error Estimates for the Combined h and p Versions of the Finite Element Method," Numer. Math., vol. 37, pp.257-277 (1981)

[7] Ghaddar, N.K., Korczak, K.Z., Mikic, B.B., and Patera, A.T., "Numerical Investigation of Incompressible Flow in Grooved Channels. Part 1. Stability and Self-Sustained Oscillations," Journal of Fluid Mechanics, vol. 163, pp. 99-127 (1986)

[8] Ronquist, Einar M., Ph.D. Thesis, Massachusetts Institute of Technology (1988)

[9] Batchelor, G.K., An Introduction to Fluid Dynamics, Cambridge University Press, Cambridge, Great Britain (1988)

[10] Durst, F., Ernst, F., and Pereira, J.C.F., "LDA Measurements of Time Dependant, Separated, Internal Flows," International Symposium on Applications of Laser Doppler Anemometry to Fluid Mechanics, Lisbon, Portugal (1982)

[11] Tjan, Wasi, "Quantitative Flow Visualization," Master's Thesis Case Western Reserve University (1986)

[12] Korczak, K.Z., Wessel R., "Mixing Control in a Plane Shear Layer", AIAA Journal, December 1989.

[13] Eisenberg, Philip, "Research Trends in Naval Hydrodynamics ... The ONR Program," Journal of Ship Research, vol. 2, no. 1, pp. 3-7 (1958)

[14] McVoy, James L., "Prediction of a Submarine's Trajectory by an Approximate Solution of its Equations of Motion," Naval Engineers Journal, vol. 91, no. 4, pp. 19-42 (1979)

[15] Reid, Walter P., "On the Motion of a Missile Under Water," Jet Propulsion, vol. 26, no. 6, pp. 463-464 (1957)

[16] May, Albert, "Review of Water-Entry Theory and Data," Journal of Hydrodynamics, vol. 4, no. 4, pp.140-142 (1970)

[17] Moran, John P., "The Vertical Water-Exit and -Entry of Slender Symmetric Bodies," Journal of the Aerospace Sciences, vol. 28, no. 10, pp. 803-812 (1961)

[18] Wislicenus, George F., "Hydrodynamics and Propulsion of Submerged Bodies," ARS Journal, vol. 30, no.12, pp. 1140-1148 (1960)

[19] Berdichevskii, V.L., "On the Force Acting on a Body in Viscous Fluid," Applied Mathematics and Mechanics, vol. 45, no. 5, pp. 628-631 (1981)

[20] Fuhrman, R.A., "The Fleet Ballistic Missile System: Polaris to Trident," Journal of Spacecraft and Rockets, vol. 15., no. 5, pp. 265-286 (1978)

[21] Morrison, J.R., O'Brien, M.P., Johnson, J.W. and Schaaf, S.A., "The Forces Exerted by Surface Waves on Piles," Journal of Petroleum Technology, vol. 189, p. 149 (1950)

[22] Hamann, F.H. and Dalton, C., "The Forces on a Cylinder Oscillating Sinusoidally in Water," Journal of Engineering for Industry, pp. 1197-1202 (1971)

[23] Sarpkaya, Turgut, "Force on a Circular Cylinder in Viscous Oscillatory Flow at Low Keulegan-Carpenter Numbers," Journal of Fluid Mechanics, vol. 165, pp. 61-71 (1986)

[24] Keulegan, G.H. and Carpenter, L.H., "Forces on Cylinders and Plates in an Oscillating Fluid," United States Bureau of Standards - Journal of Research, vol. 60, no. 5, pp. 423-440 (1958)

[25] Williamson, C.H.K., "Sinusoidal Flow Relative to Circular Cylinders," Journal of Fluid Mechanics, vol. 155, pp. 141-174 (1985)

[26] Tatsuno, M. and Bearman, P.W., "A Visual Study of the Flow Around an Oscillating Circular Cylinder at Low Keulegan-Carpenter Numbers and Low Stokes Numbers," Journal of Fluid Mechanics, vol. 211, pp. 157-182 (1990)

[27] Hurlbut, S.E., Spaulding, M.L. and White F.M., "Numerical Solution for Laminar Two Dimensional Flow About a Cylinder Oscillating in a Uniform Stream," Journal of Fluids Engineering, vol. 104, pp. 214-222 (1982)

[28] Bratanow, Theodaore, Ecer, Akin, and Kobiske, Micheal, "Finite Element Analysis of Unsteady Incompressible Flow Around an Oscillating Obstacle of Arbitrary Shape," AIAA Journal, vol. 11, no. 11, pp. 1471-1477 (1973)

[29] Sorokodum, E.D., "Flow Near a Vibrating Cylinder," Fluid Dynamics, vol. 17, no. 4, pp. 654-656 (1982)

List of Figures

Figure 12(a-c). Velocity vectors for the two-dimensional cylinder oscillating at an amplitude equal to 2.0*radius. Sine curves at the top of each figure identify the location of the cylinder in the cycle.

Figure 13(a-c). Pressure for the two-dimensional cylinder oscillating at an amplitude equal to 1.0*radius (opened arrows indicate negative pressure, closed arrows indicate positive pressure). Sine curves at the top of each figure identify the location of the cylinder in the cycle.

Figure 14. Computational domain for the three-dimensional oscillating cylinder. Only element edges are plotted for clarity.

Figure 15. Forces and moments recorded on the three-dimensional oscillating cylinder at a Reynolds number of 120.

Figure 16. Schematic drawing of the separating objects configuration.

Figure 17. Plots of velocity vectors and pressure for the separating objects case for theta equal to 60 degrees. (Plots are for flow after 100 time steps of simulation.)

Figure 18. Plots of velocity vectors and pressure for the separating objects case for theta equal to zero degrees. For pressure, open arrows indicate negative pressure, closed arrows indicate positive pressure, the length of the arrows is proportional to pressure magnitude. (Plots are for flow after 100 time steps of simulation.)

Figure 19. Example of the motion of the object in the z-direction. Elements in the figure on the left are in the unstretched position. The right figure shows the object in the silo with elements stretched to accommodate that position.

Figure 20. Flow field created by an object moving in the y-direction as shown at the top of the figure. Velocity vectors and pressure are plotted next to it. For pressure, open arrows indicate negative pressure, closed arrows indicate positive pressure, the length of the arrows is proportional to pressure magnitude.

Figure 21. Plots of velocity vectors and pressure for the separating objects case with theta equal to 10 degree. For pressure, open arrows indicate negative pressure, closed arrows indicate positive pressure, the length of the arrows is proportional to pressure magnitude. (Plots represent flow field after 100 time steps of simulation.)

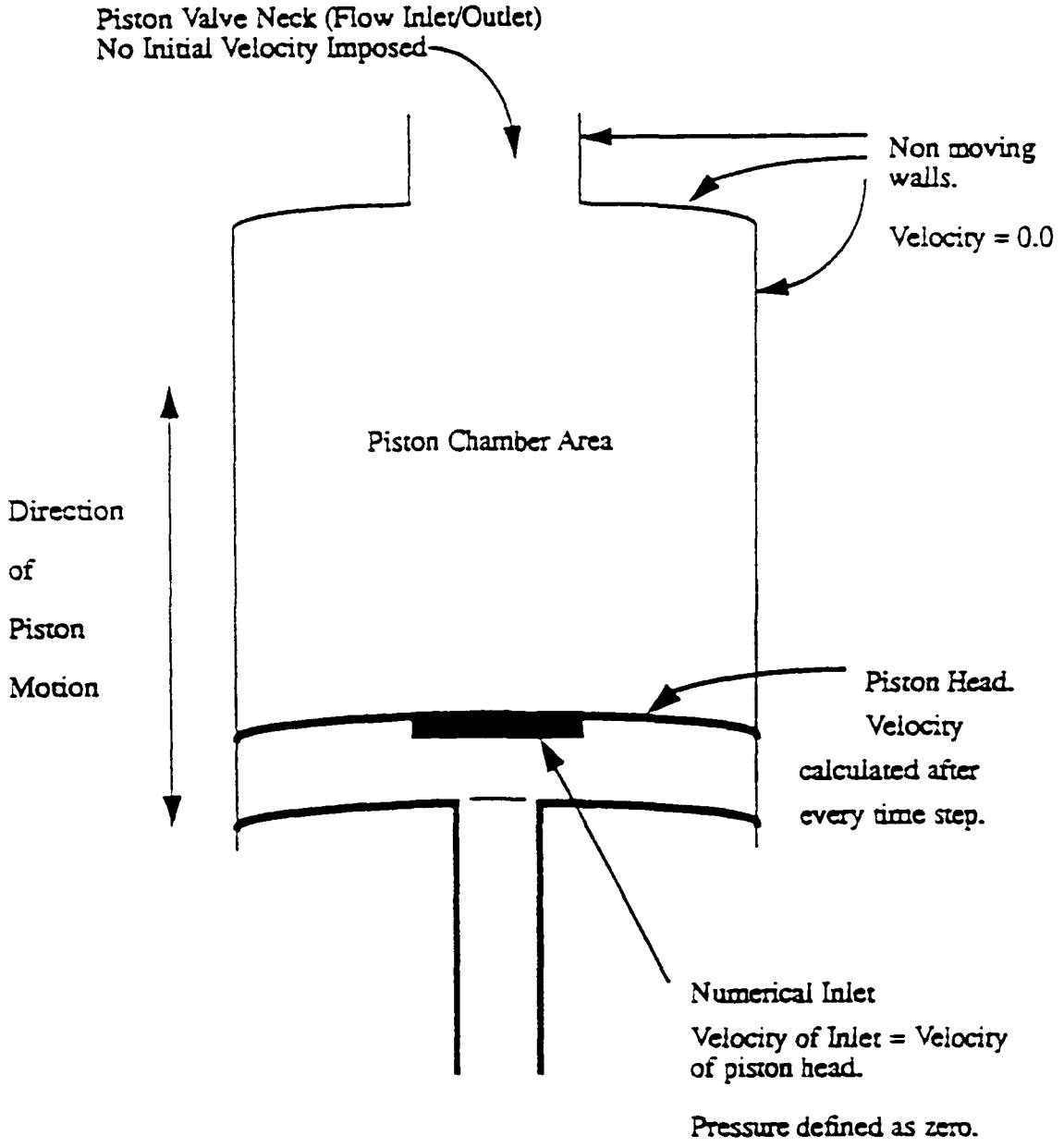

Figure 1 Schematic Drawing of the Two-Dimension Pump

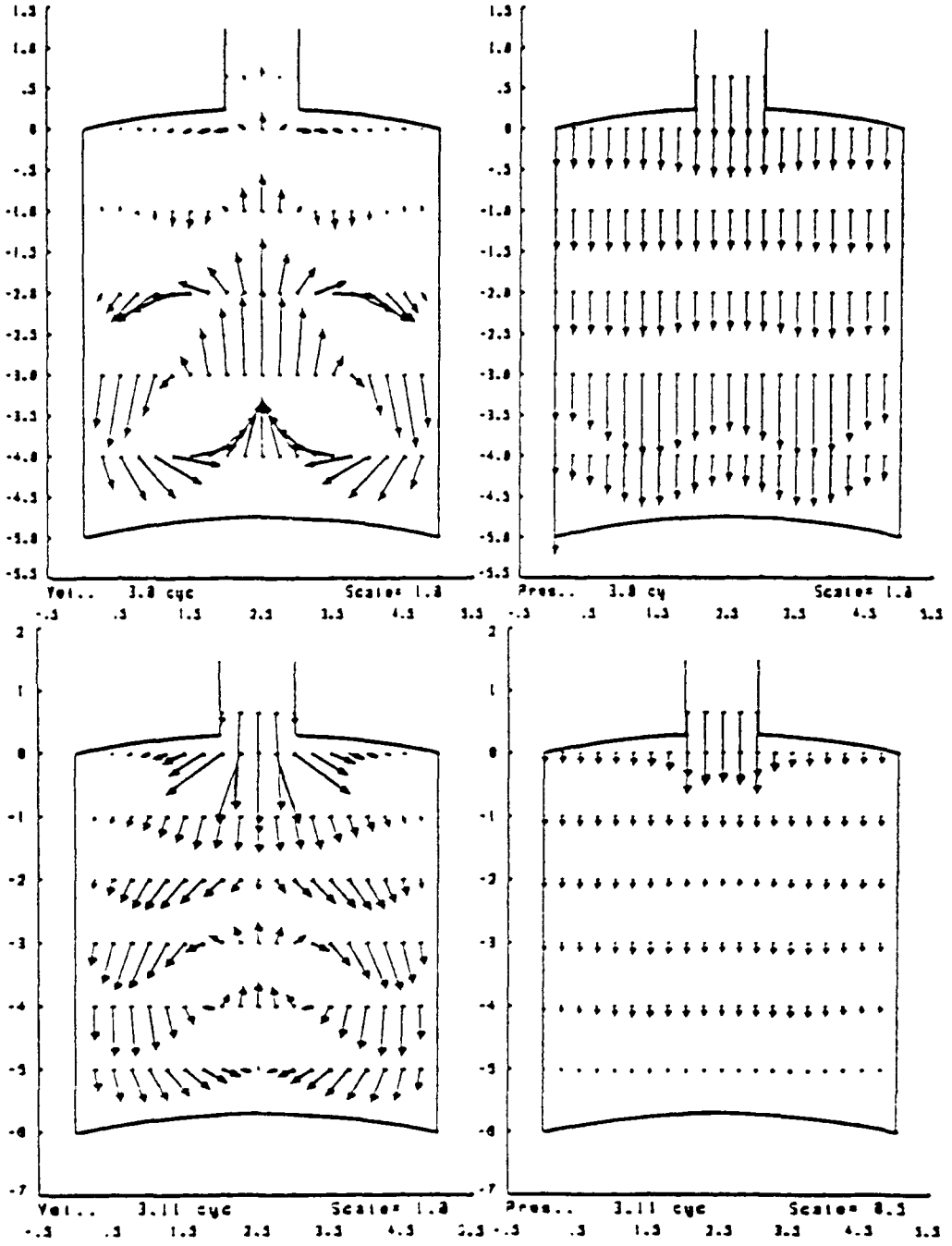

Figure 2 (a) Two-Dimensional Pump Velocity and Pressure Cycle Plots

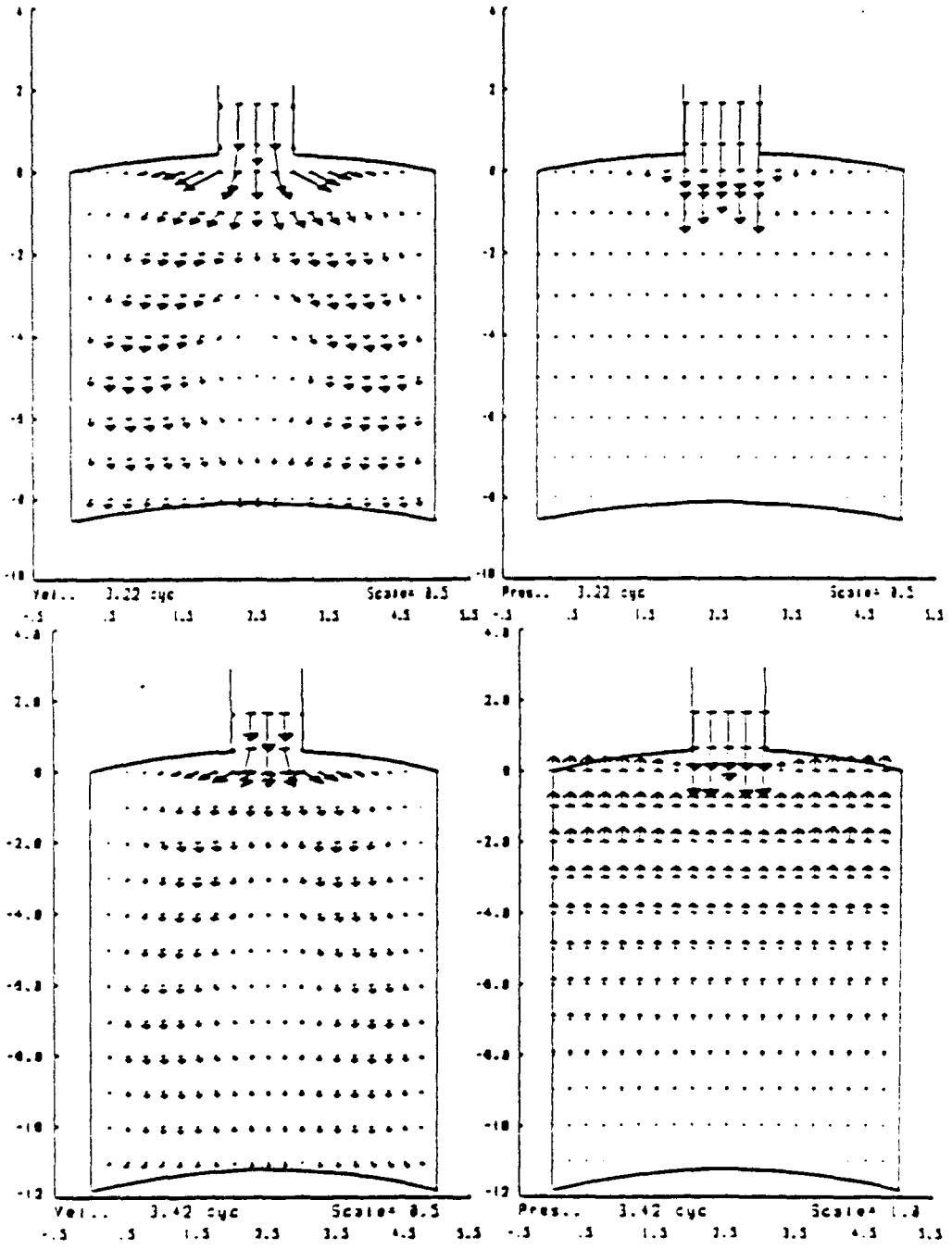

Figure 2 (b) Two-Dimensional P ump Velocity and Pressure Cycle Plots

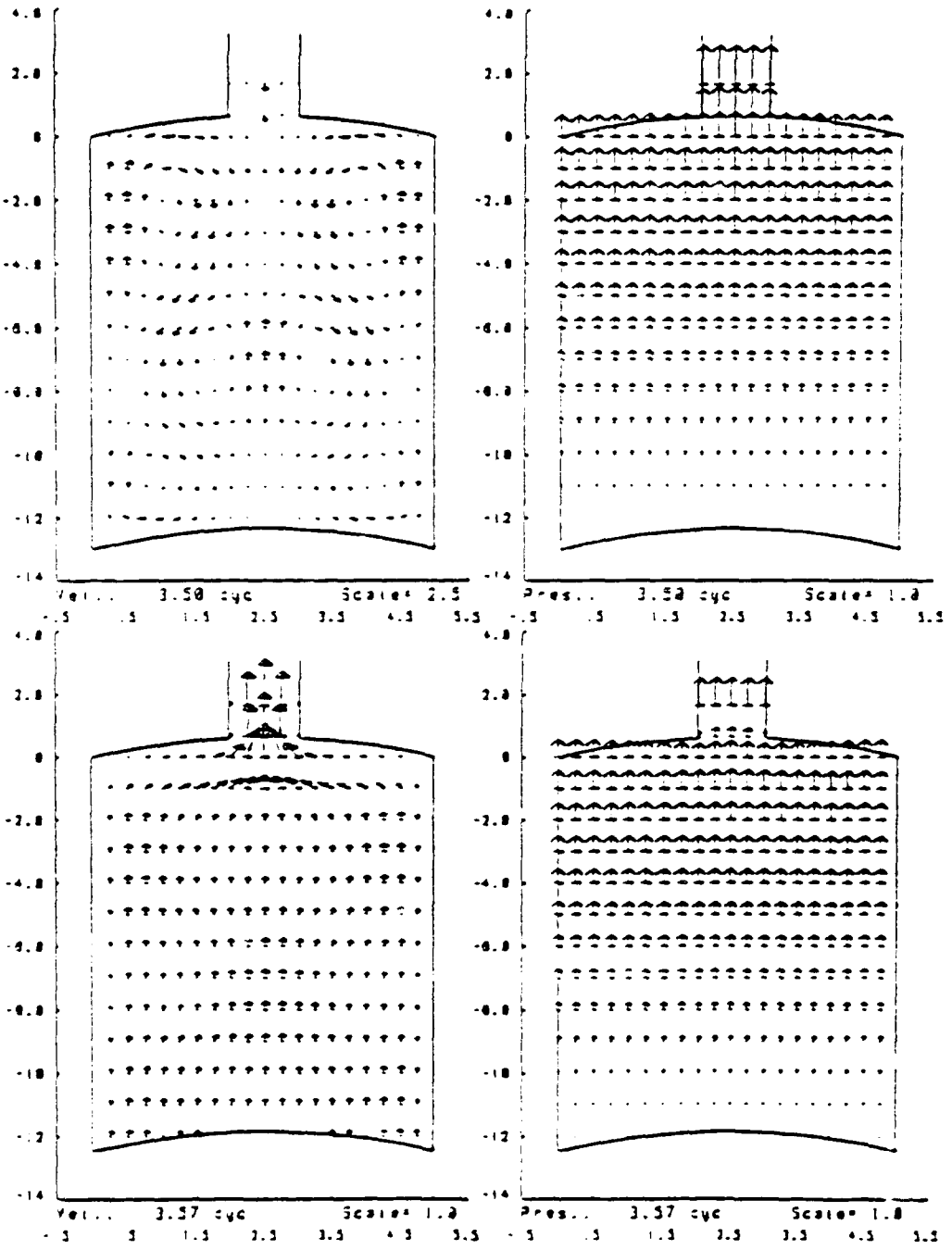

Figure 2 (c) Two-Dimensional Pump Velocity and Pressure Cycle Plots

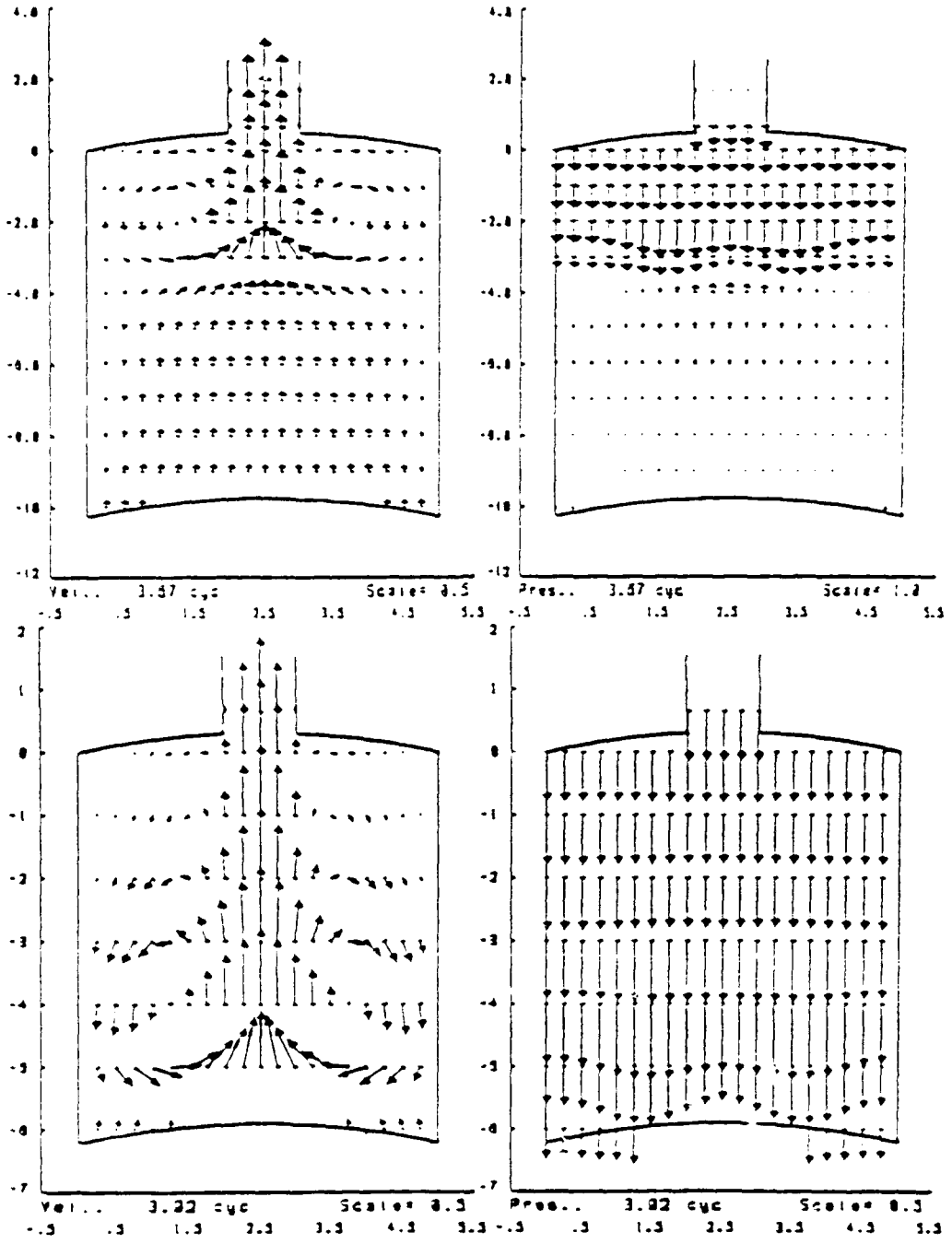

Figure 2 (d) Two-Dimensional Pump Velocity and Pressure Cycle Plots

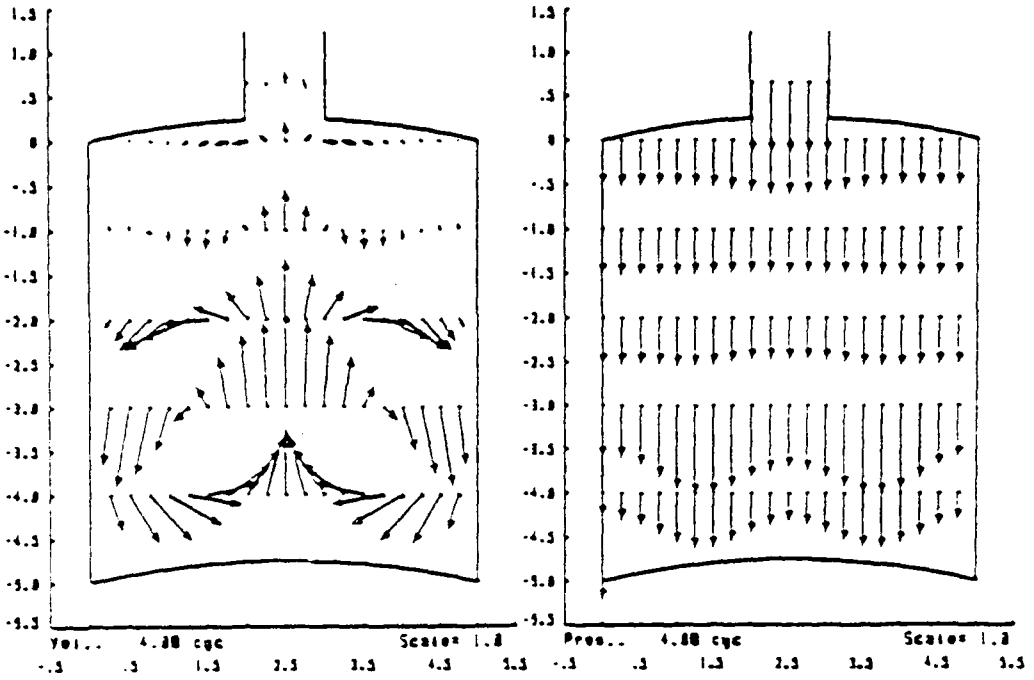

Figure 2 (e) Two-Dimensional Pump Velocity and Pressure Cycle Plots

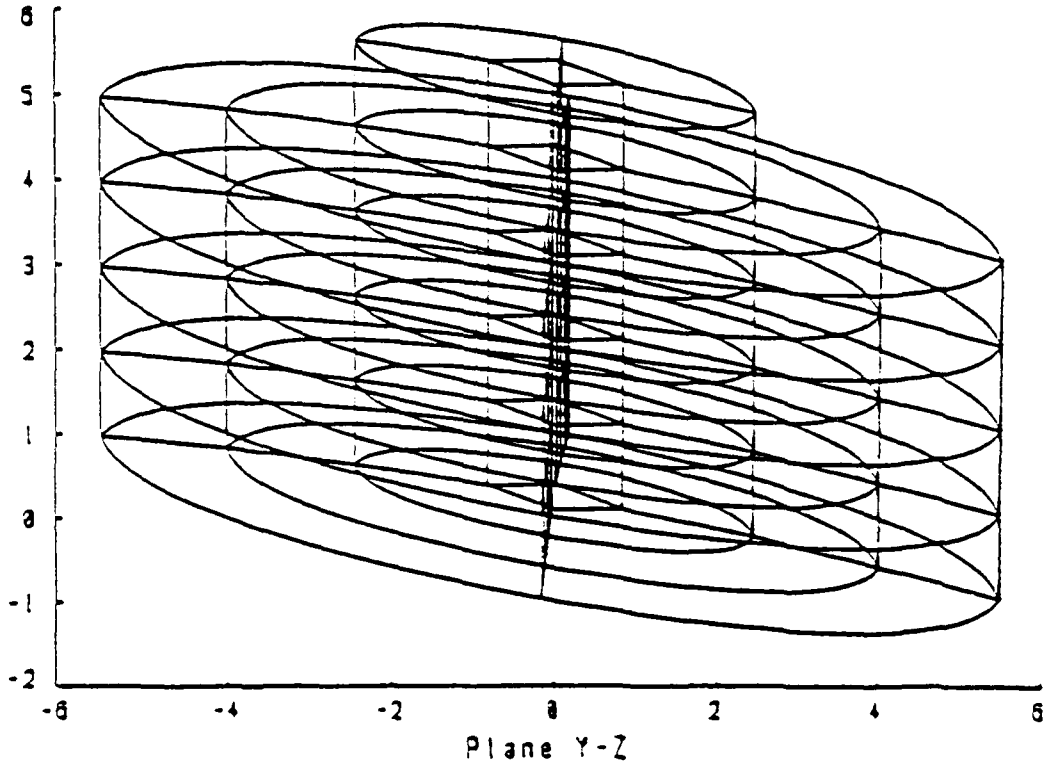

Figure 3 The Three-Dimensional Pump

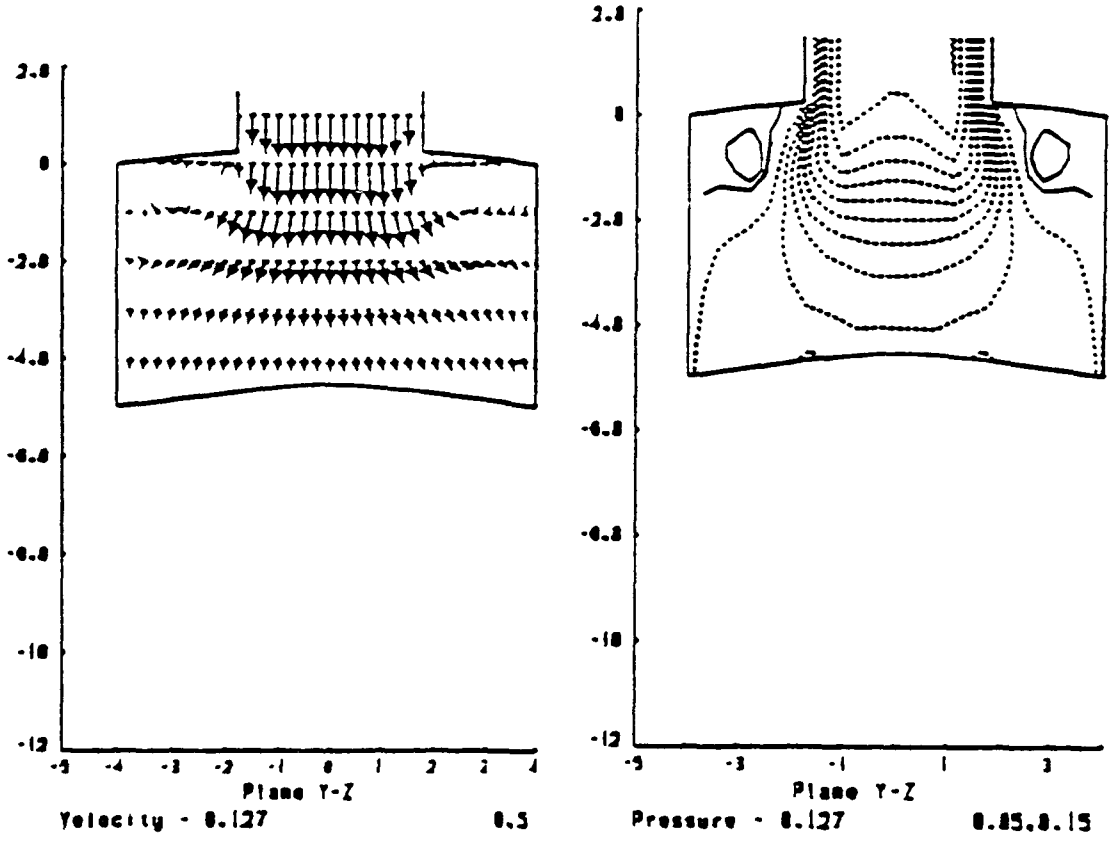

Figure 4 (a) Three-Dimensional Pump Velocity and Pressure Cycle Plots

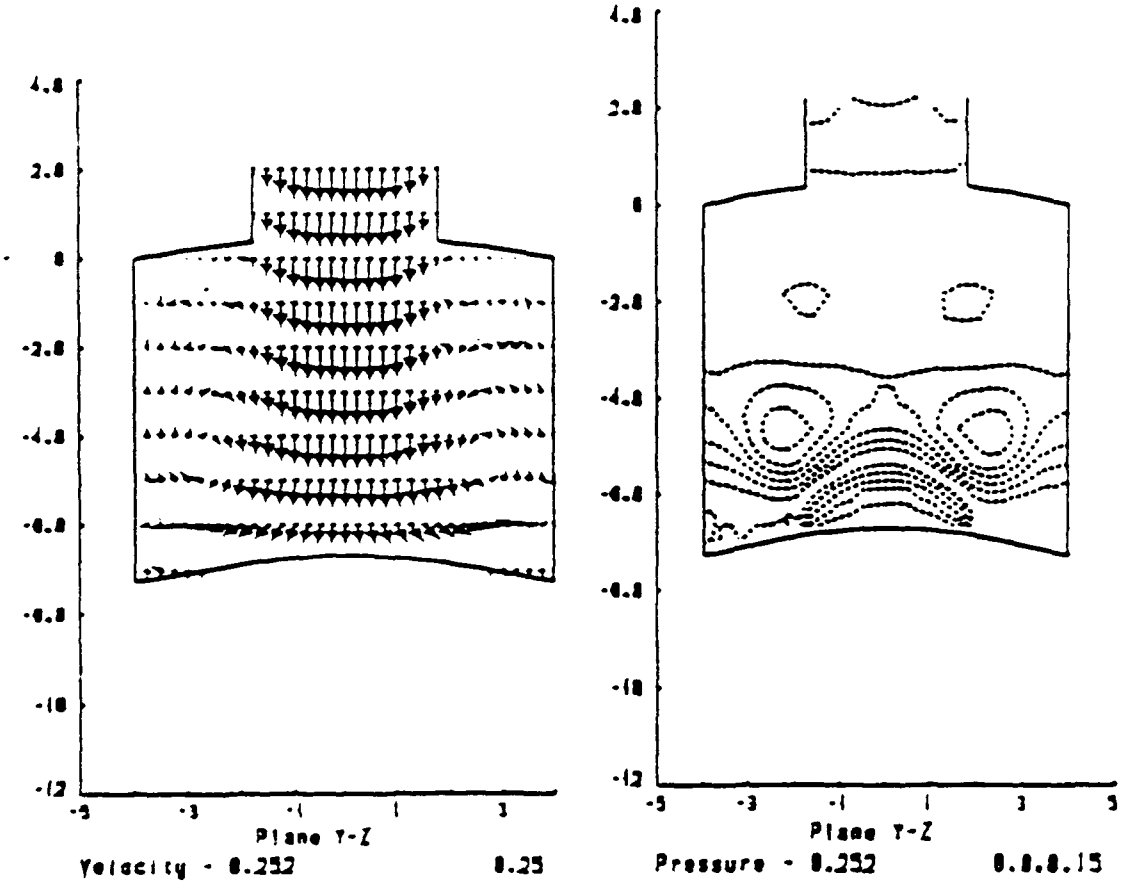

Figure 4 (b) Three-Dimensional Pump Velocity and Pressure Cycle Plots

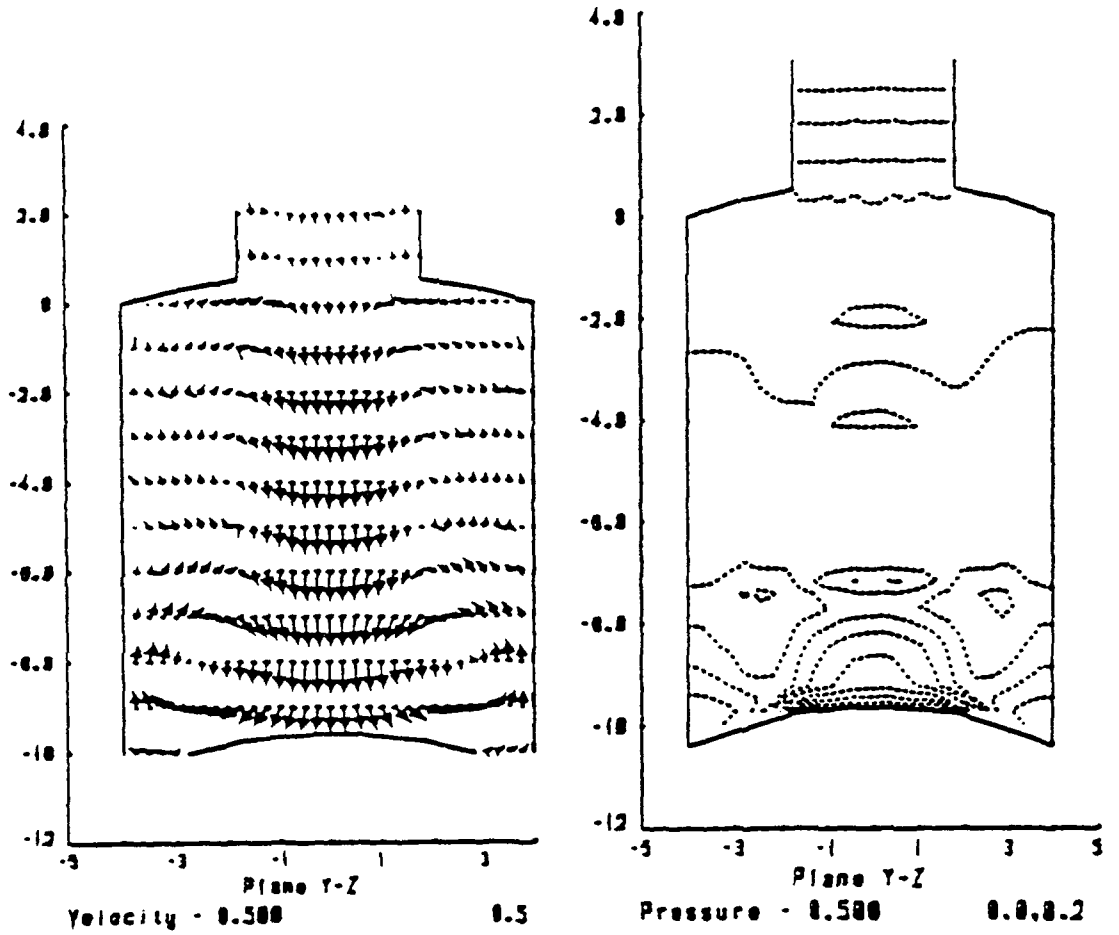

Figure 4 (c) Three-Dimensional Pump Velocity and Pressure Cycle Plots

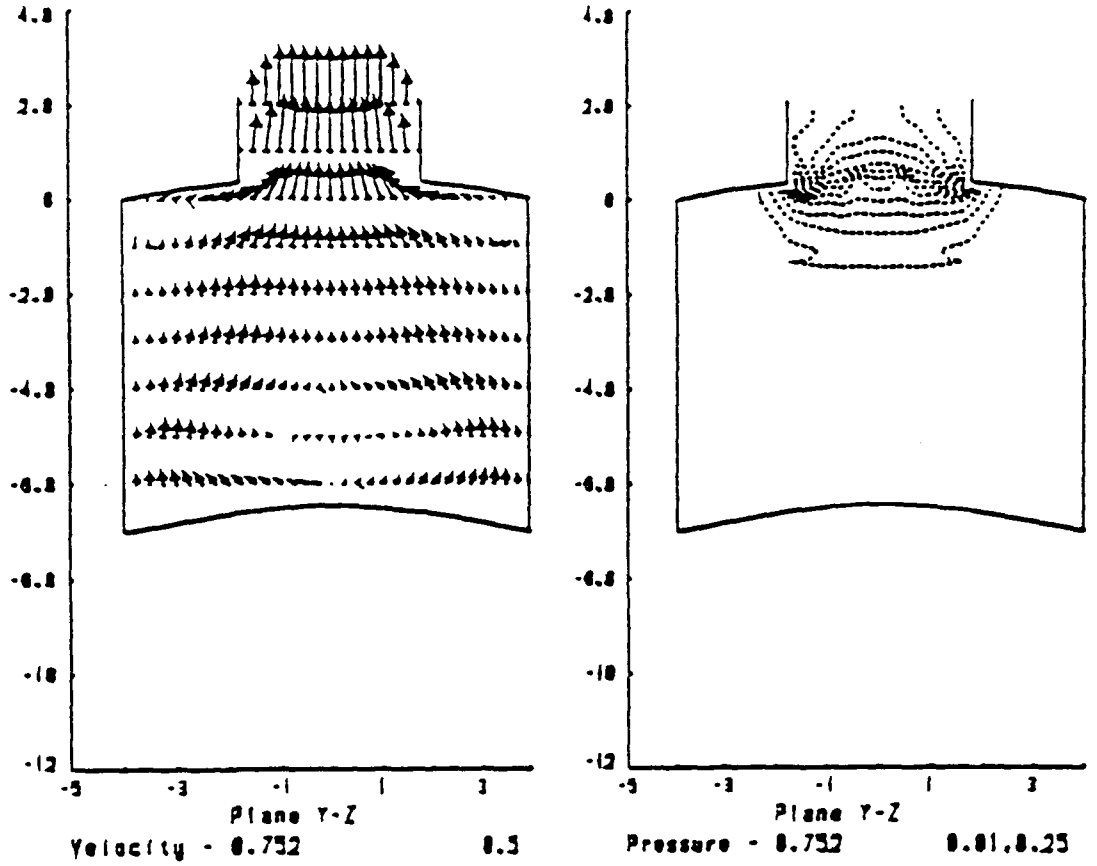

Figure 4 (d) Three-Dimensional Pump Velocity and Pressure Cycle Plots

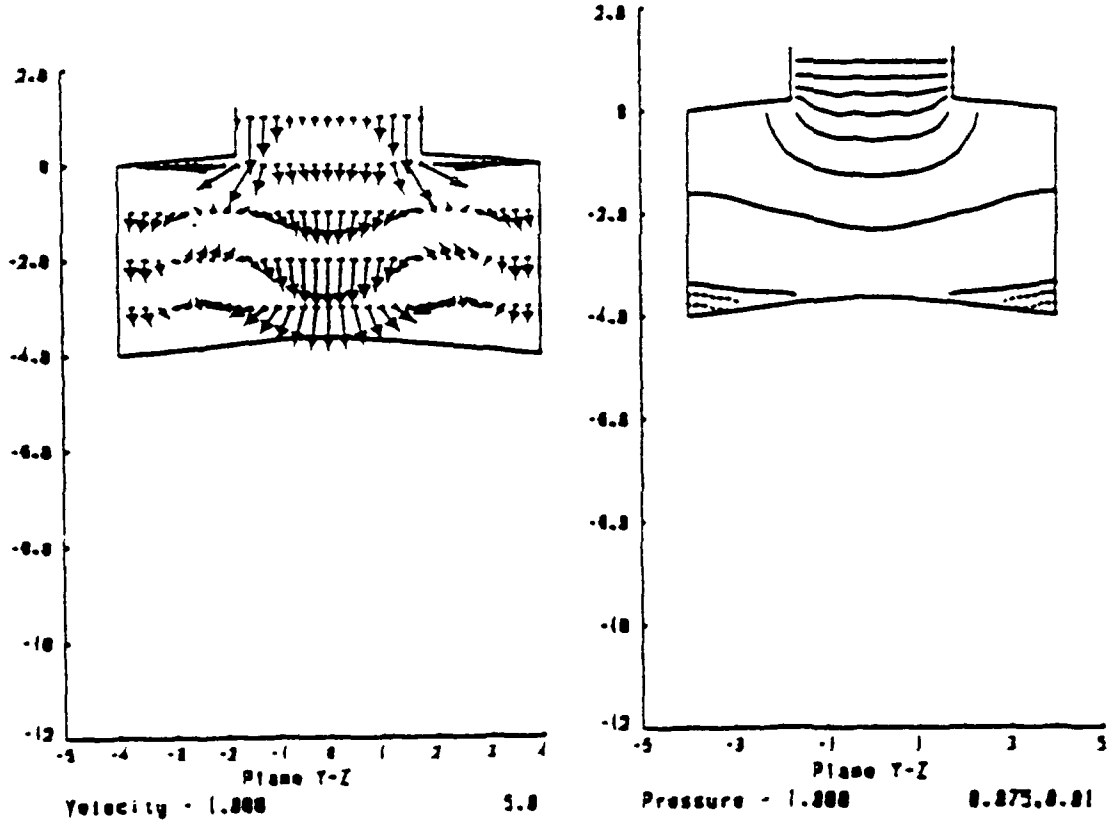

Figure 4 (e) Three-Dimensional Pump Velocity and Pressure Cycle Plots

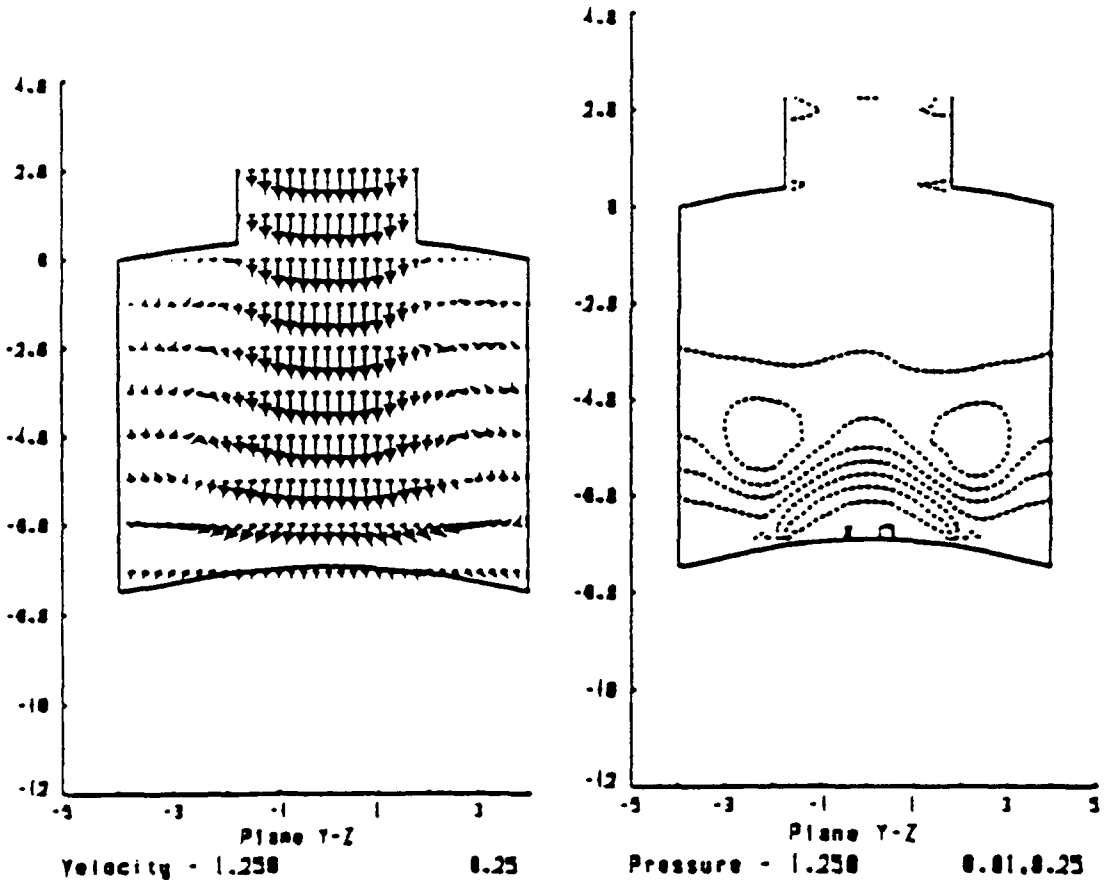

Figure 4 (f) Three-Dimensional Pump Velocity and Pressure Cycle Plots

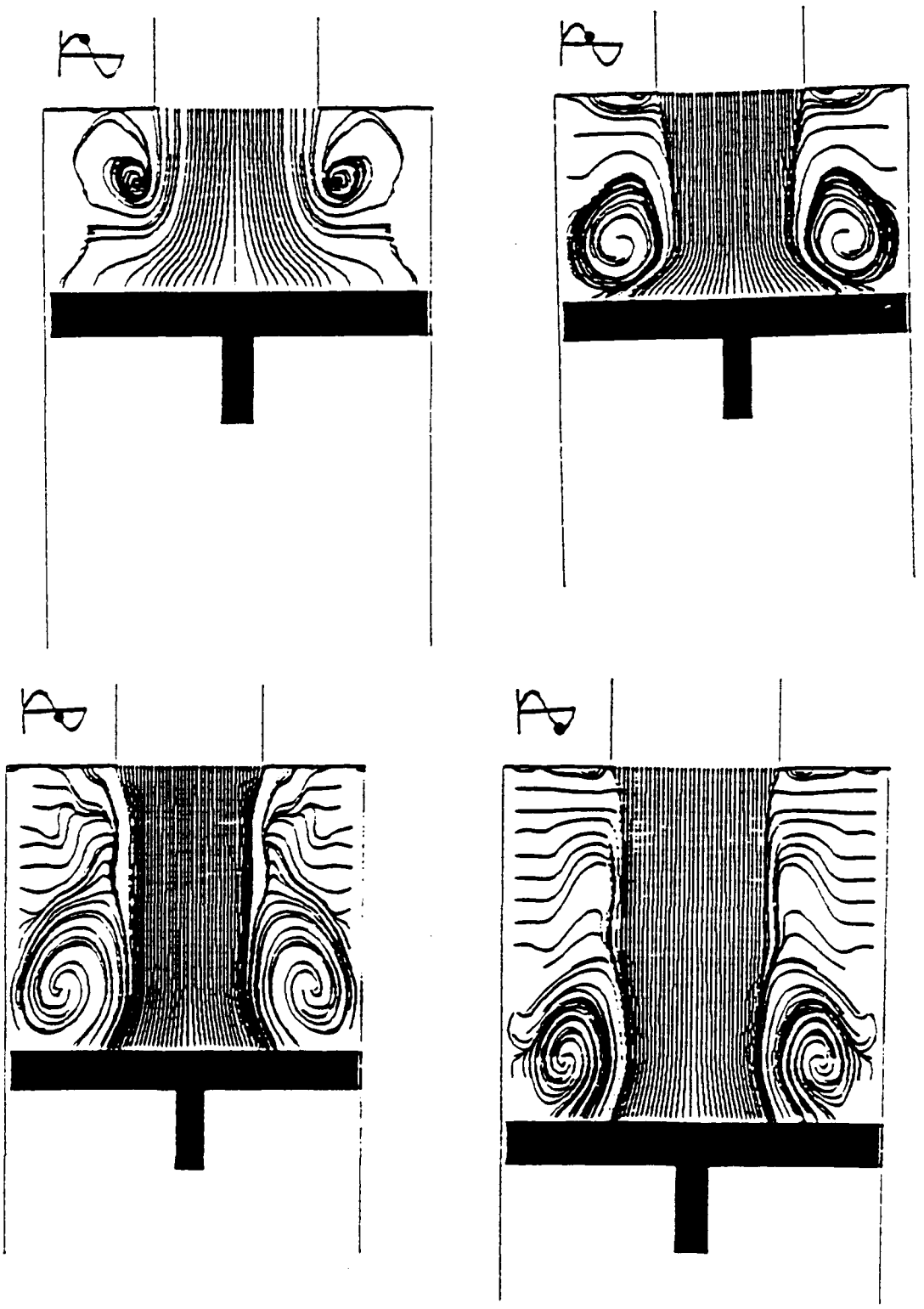

Figure 5 Experimental Pump Vorticity Plots

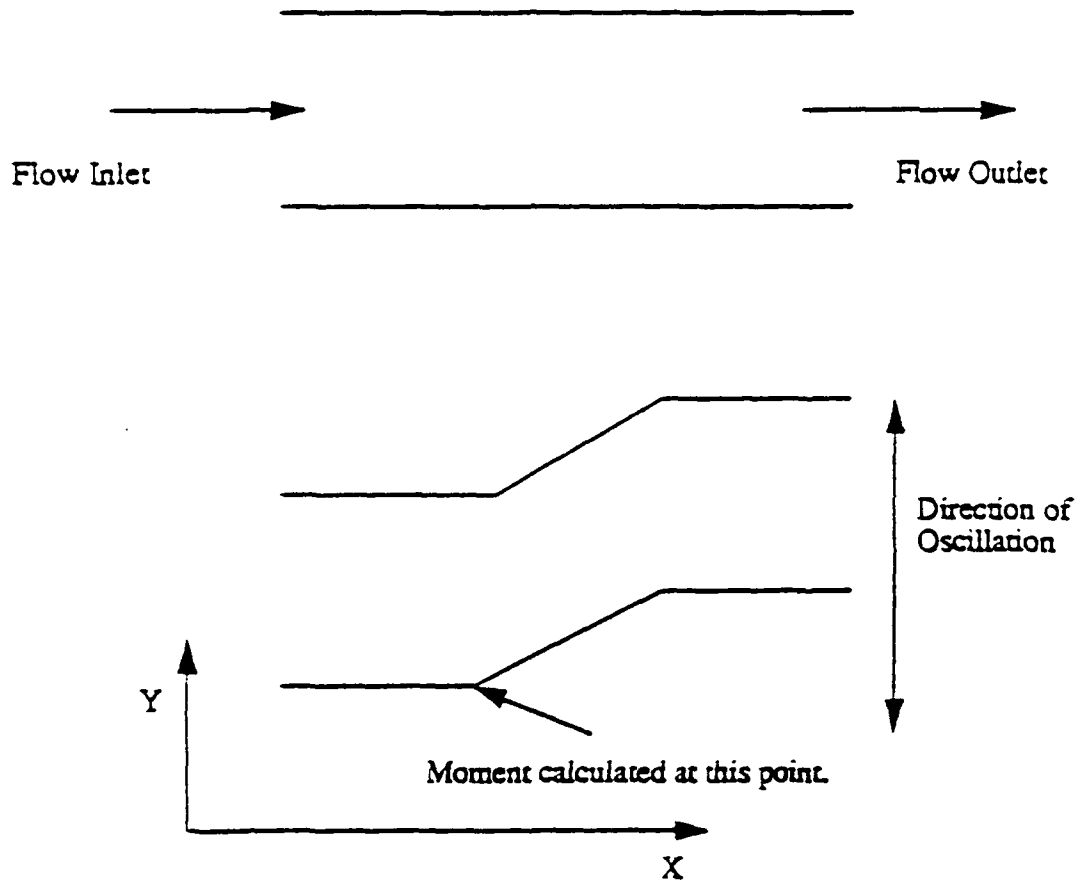

Figure 6 The Three-Dimensional Oscillating Channel

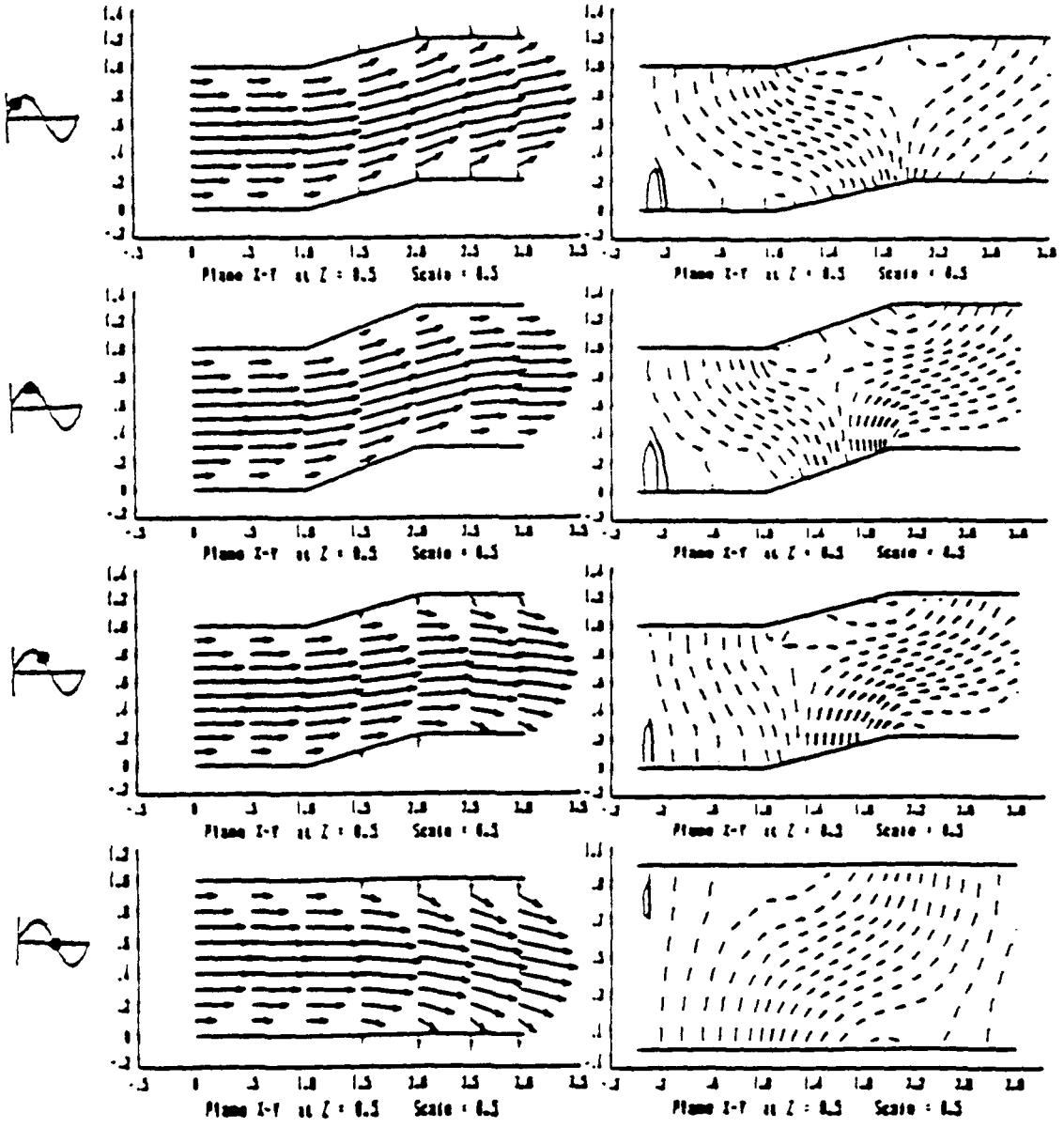

Figure 7 (a) Oscillating Channel Velocity and Pressure Plots

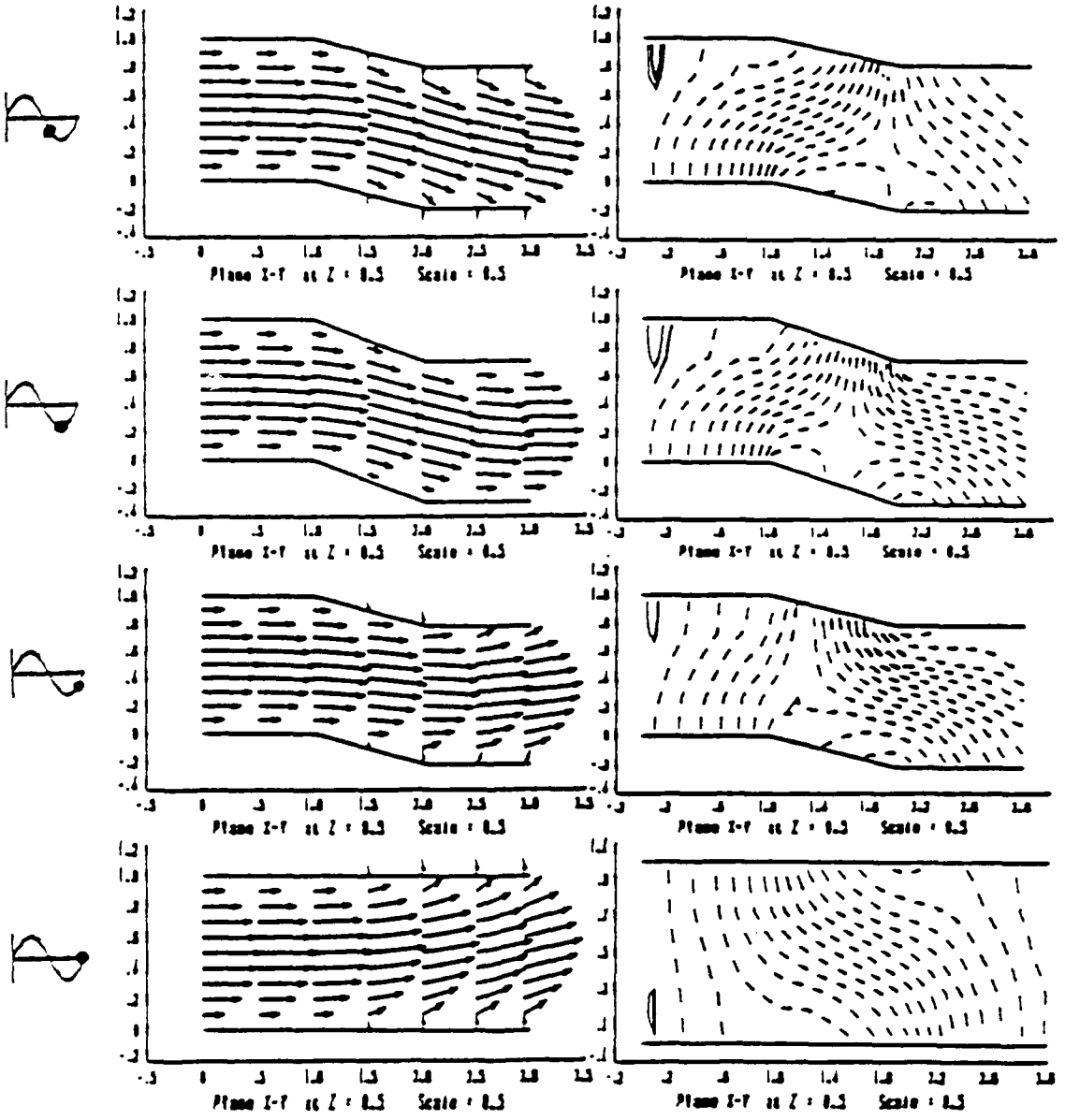

Figure 7 (b) Oscillating Channel Velocity and Pressure Plots

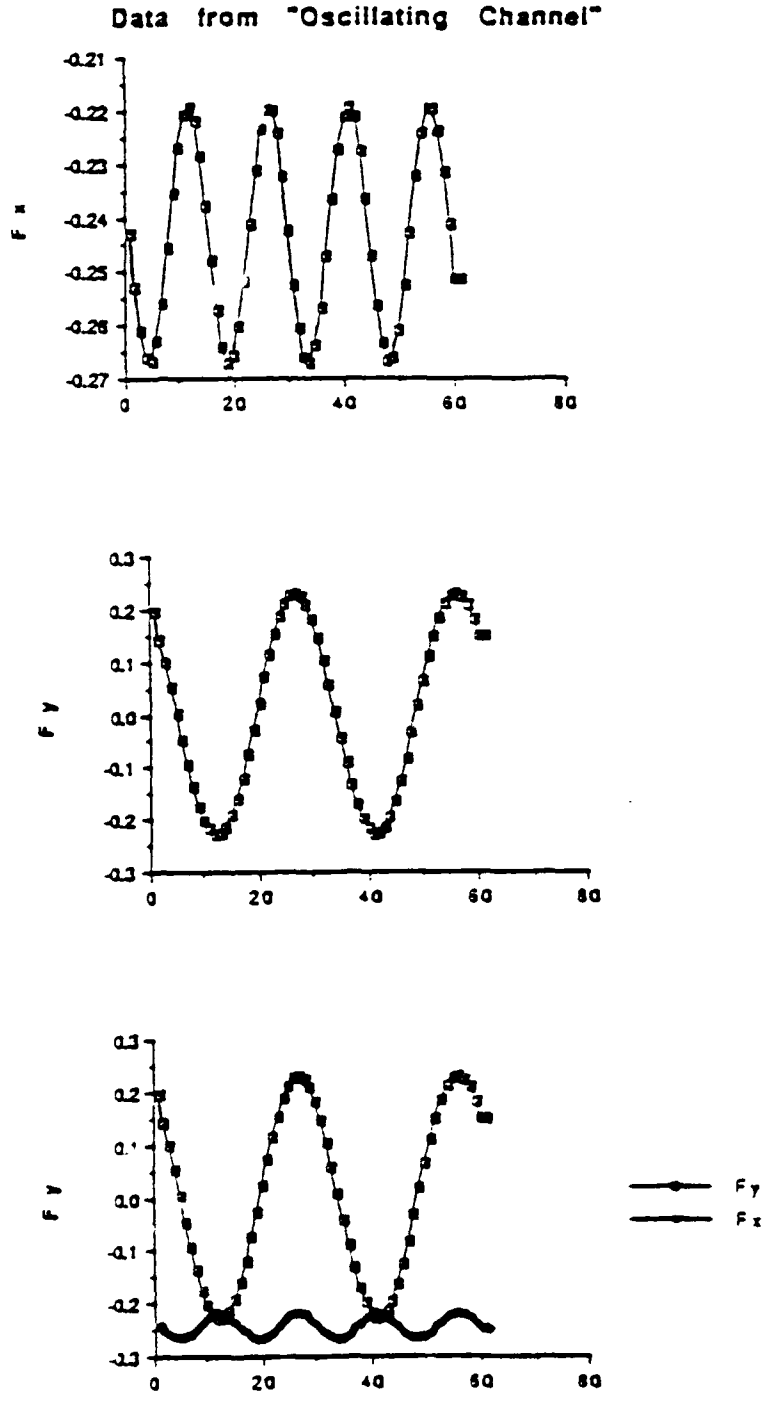

Figure 8 (a) Forces and Moments on the Oscillating Channel

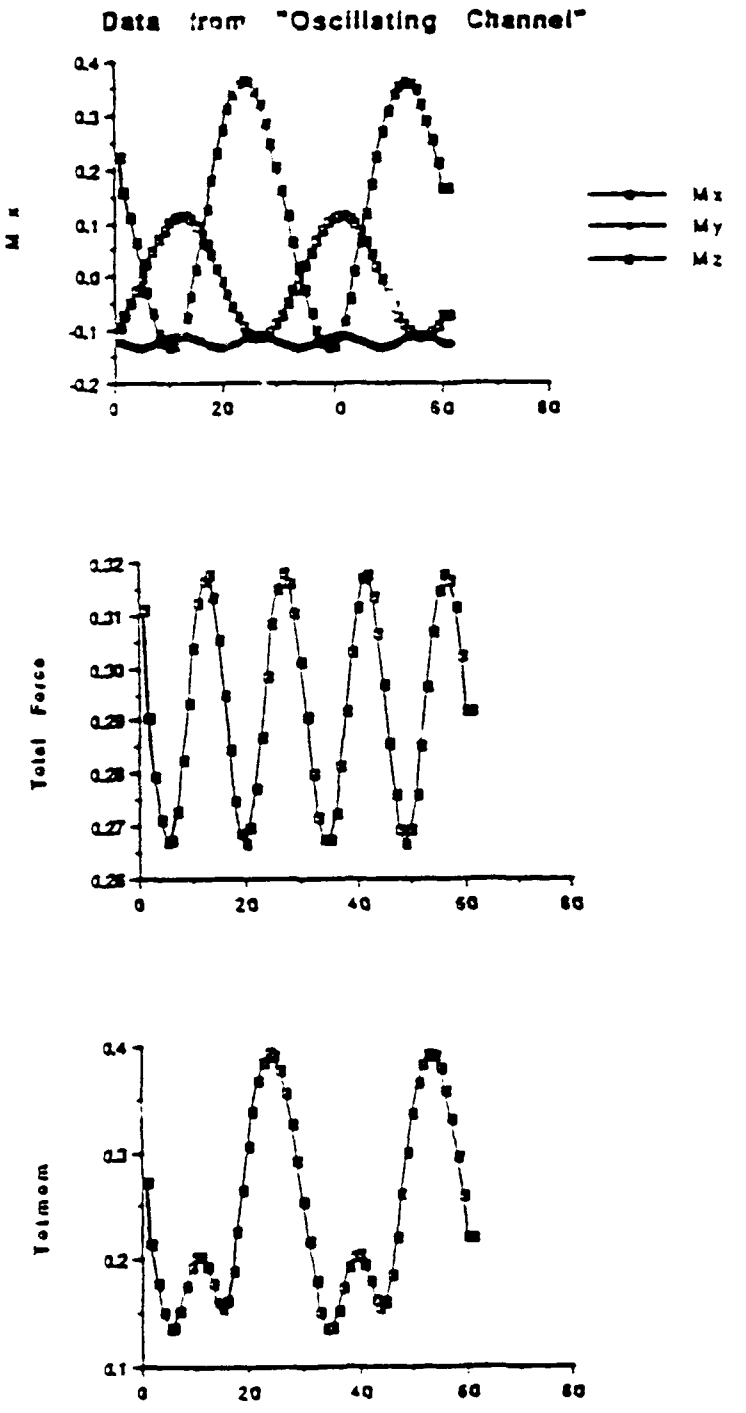

Figure 8 (b) Forces and Moments on the Oscillating Channel

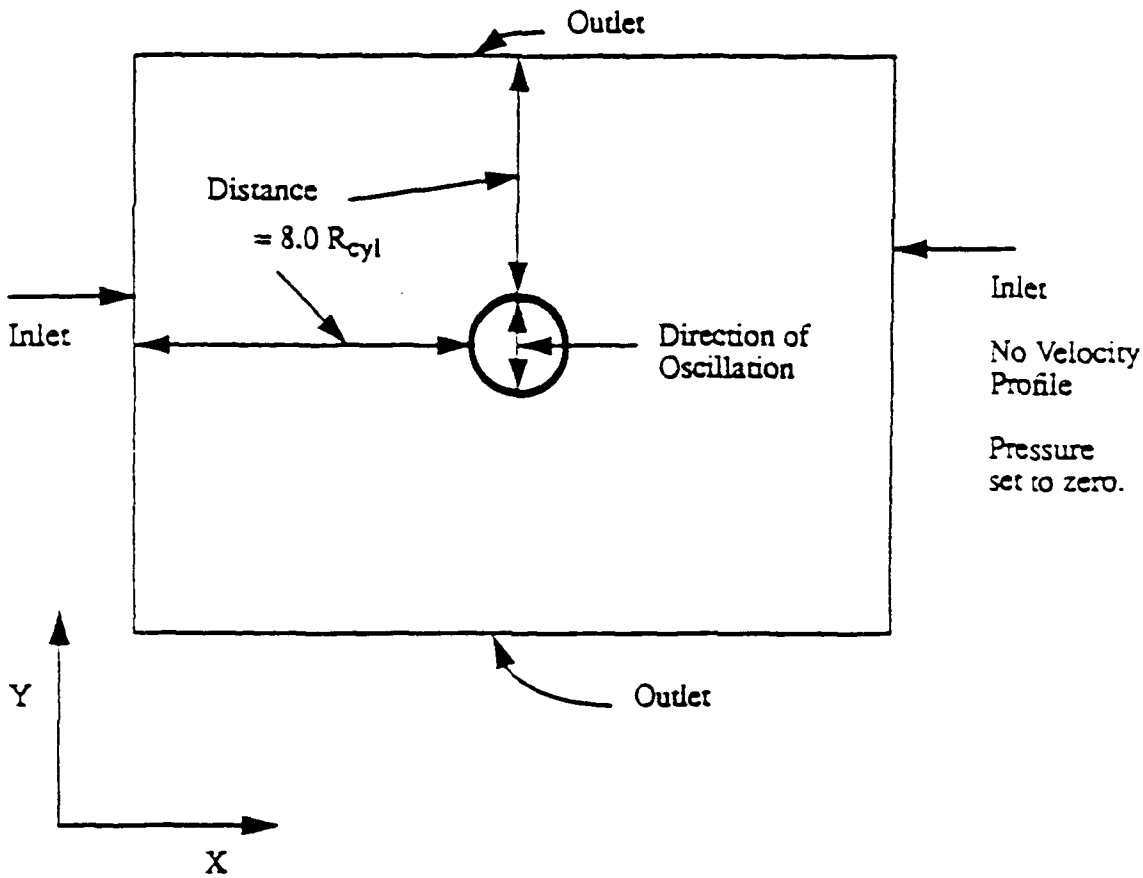

(Origin at Center of Cylinder)

Figure 9 Schematic Drawing of the Two-Dimensional Oscillating Cylinder

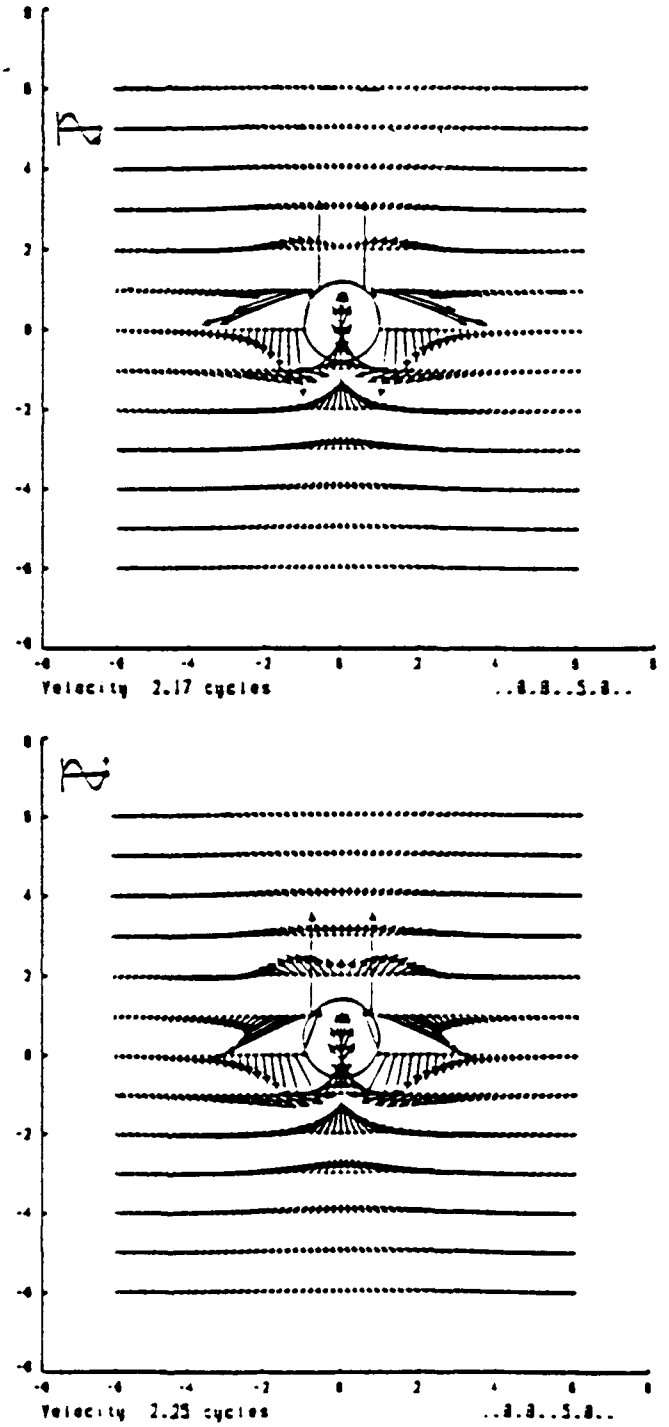

Figure 10(a) Velocity vectors for the Oscillating Cylinder (Ampl. = 0.8 Rad.)

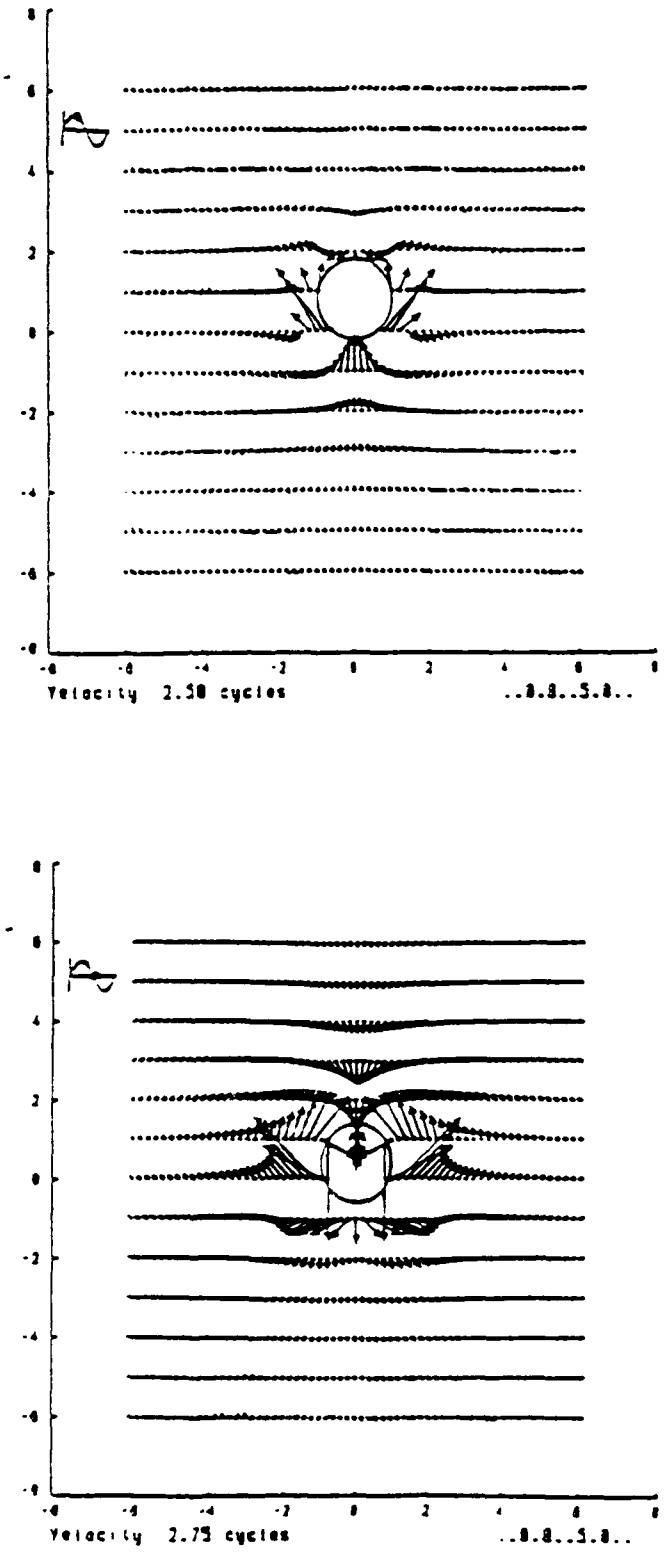

Figure 10(b) Velocity vectors for the Oscillating Cylinder (Ampl. = 0.8 Rad.)

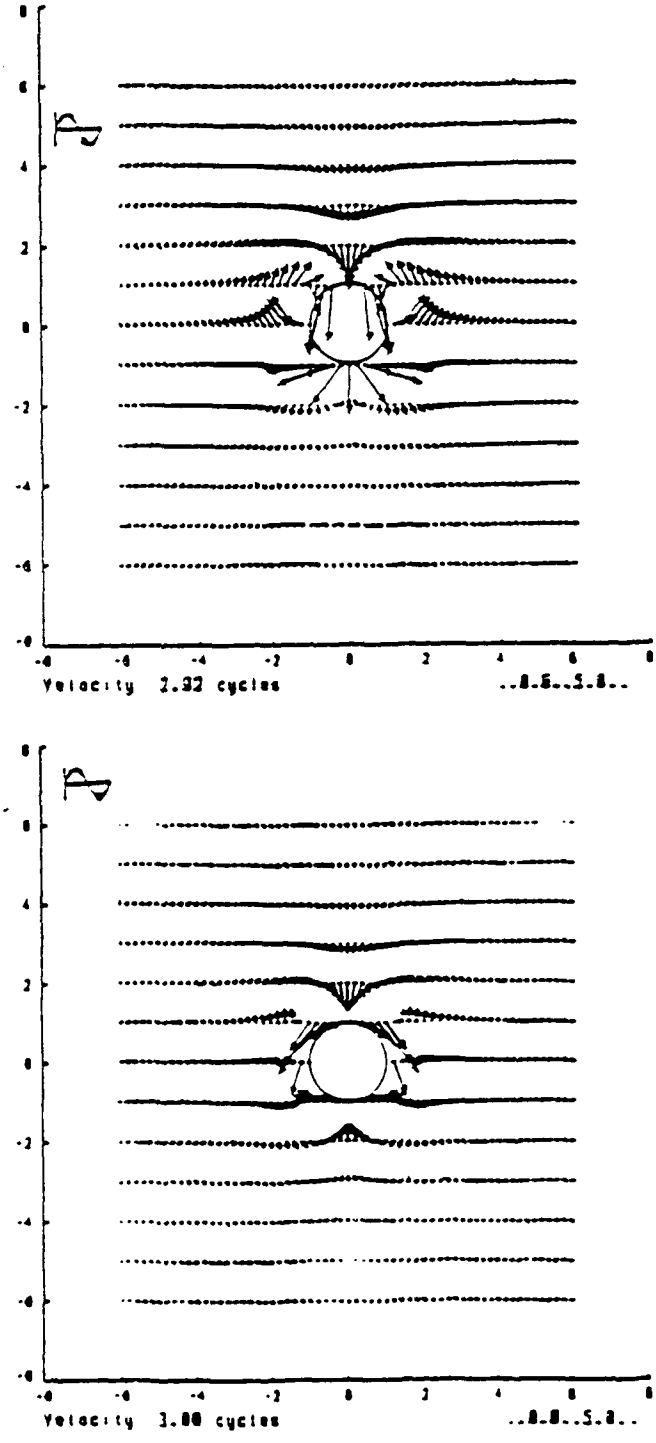

Figure 10 (c) Velocity vectors for the Oscillating Cylinder (Ampl. = 0.8 Rad.)

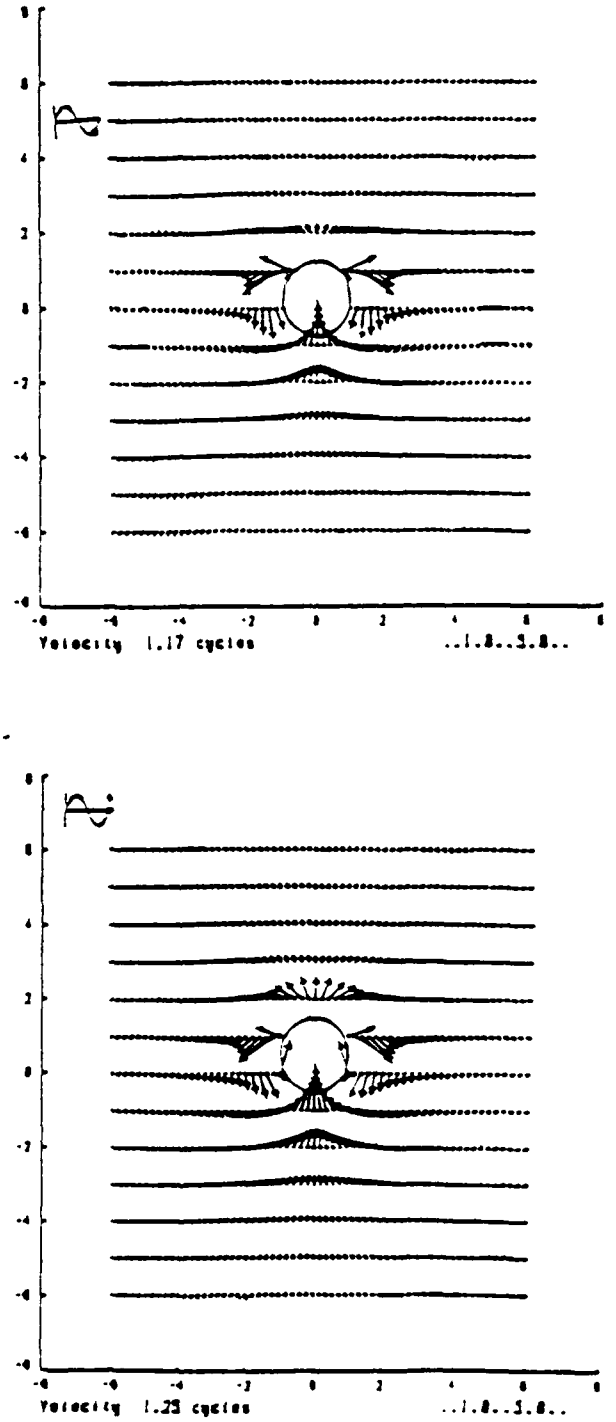

Figure 11 (a) Velocity vectors for the Oscillating Cylinder (AmpL = Rad.)

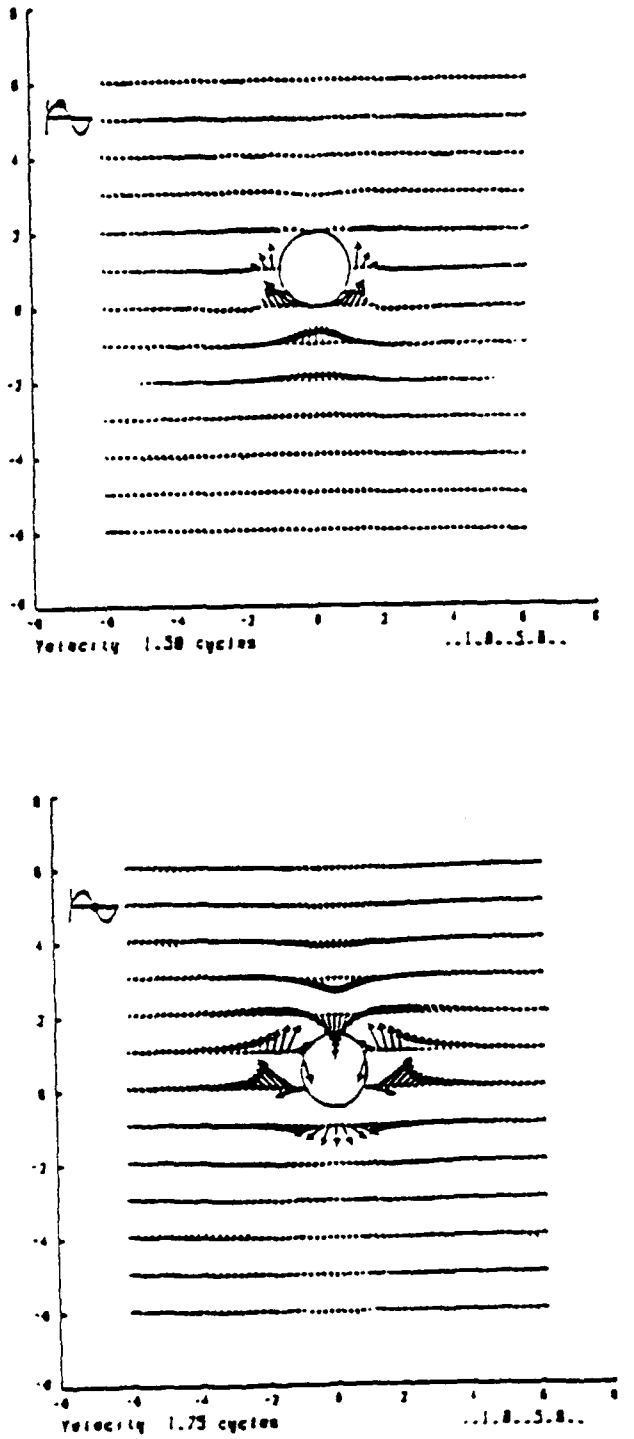

Figure 11 (b) Velocity vectors for the Oscillating Cylinder (Ampl. = Rad.)

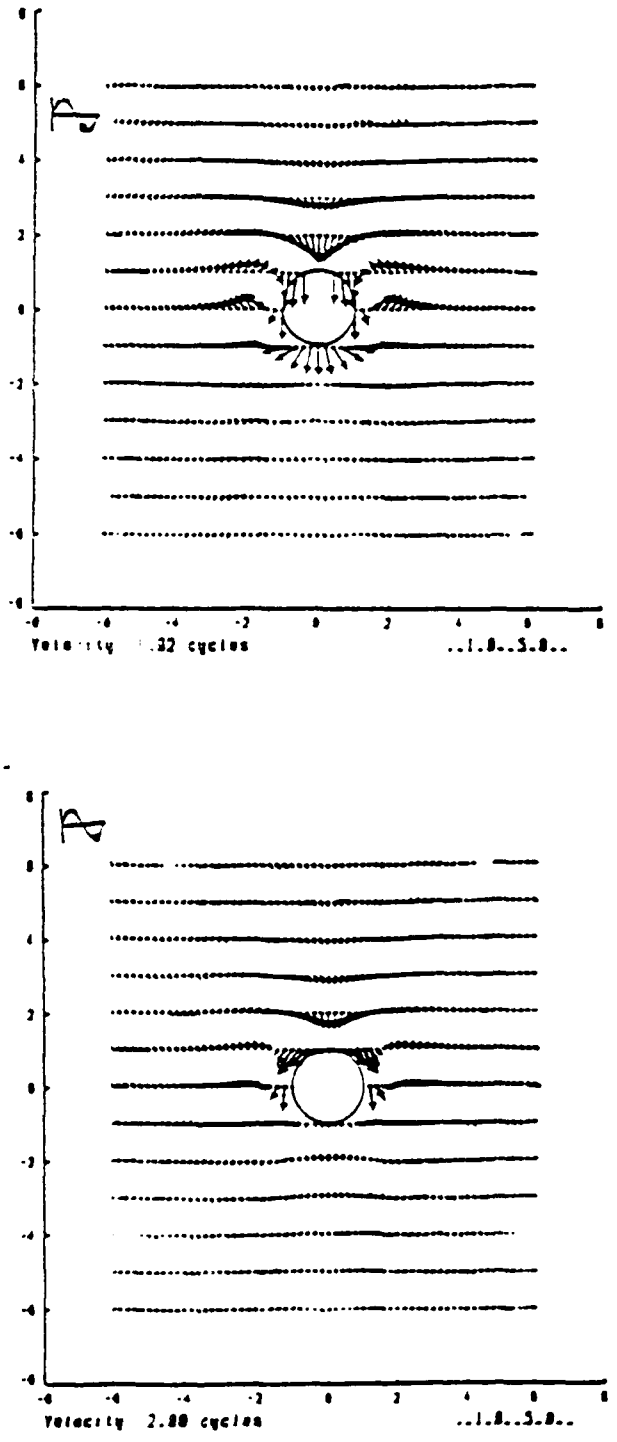

Figure 11(c) Velocity vectors for the Oscillating Cylinder (Ampl. = Rad.)

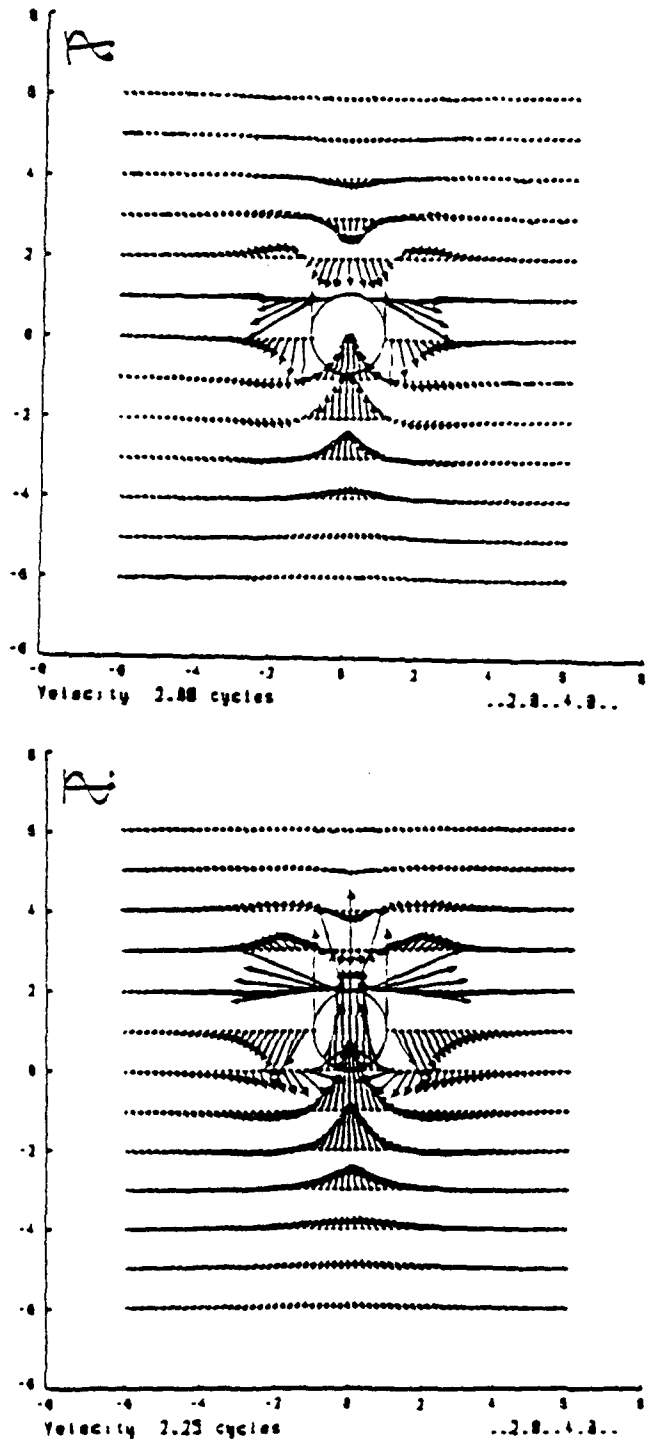

Figure 12 (a) Velocity vectors for the Oscillating Cylinder (Ampl. = 2.0 Rad.)

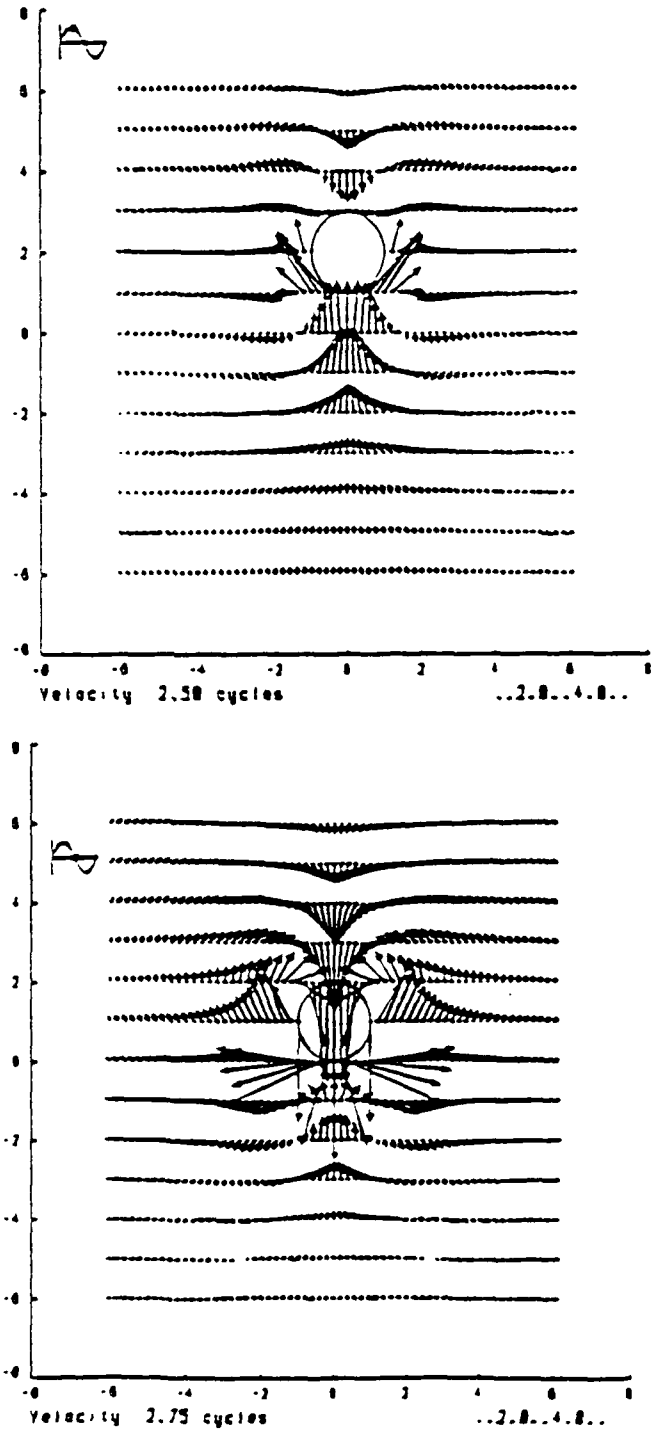

Figure 12 (b) Velocity vectors for the Oscillating Cylinder (Ampl. = 2.0 Rad.)

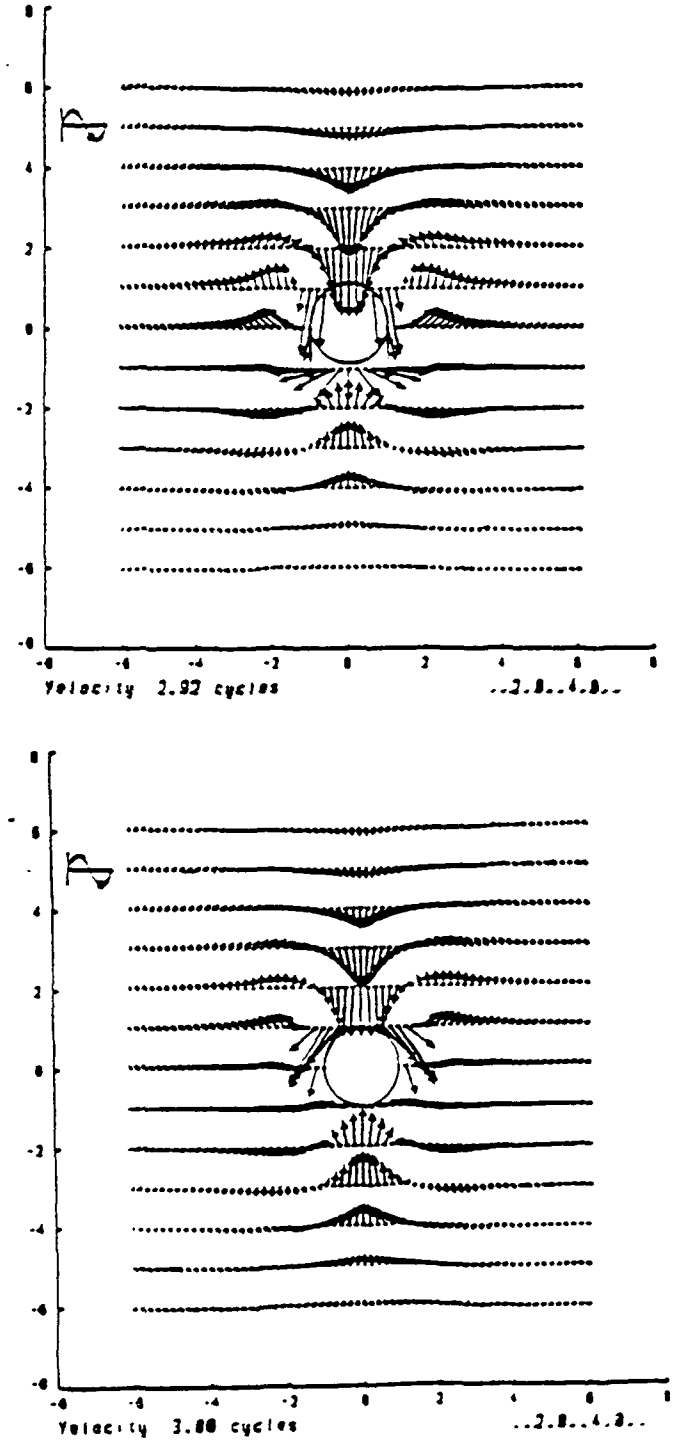

Figure 12 (c) Velocity vectors for the Oscillating Cylinder (Ampl. = 2.0 Rad.)

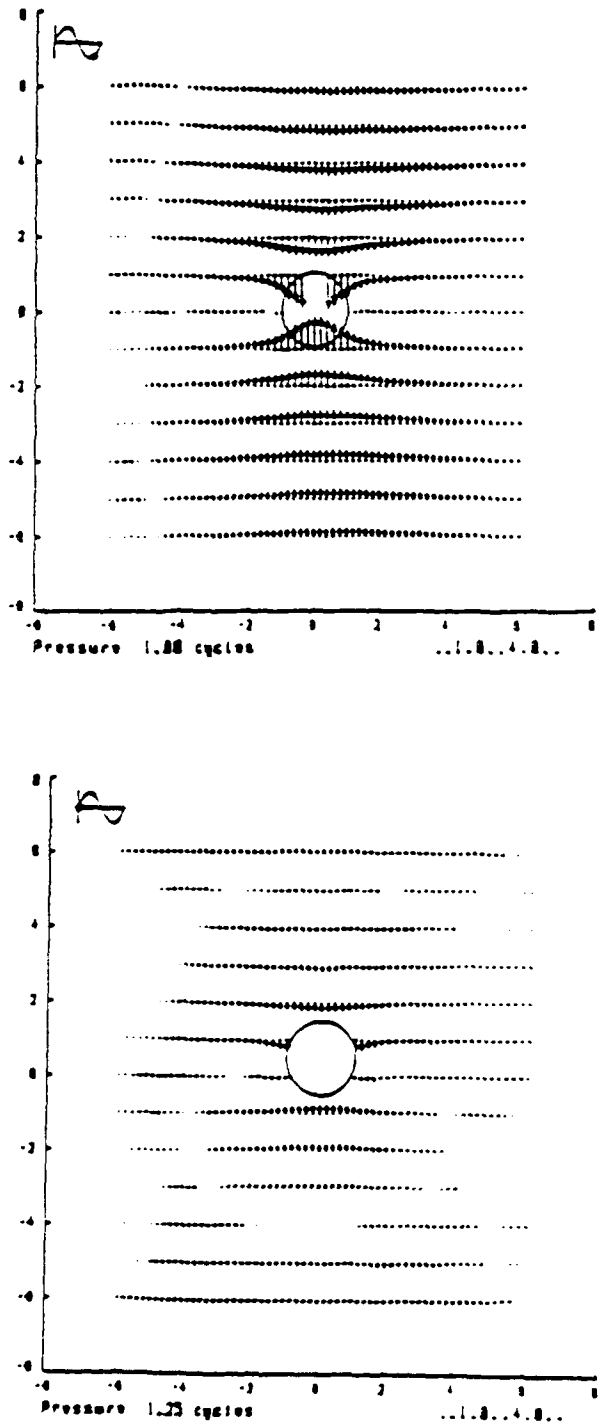

Figure 13 (a) Pressure vectors for the Oscillating Cylinder (Ampl. = Rad.)

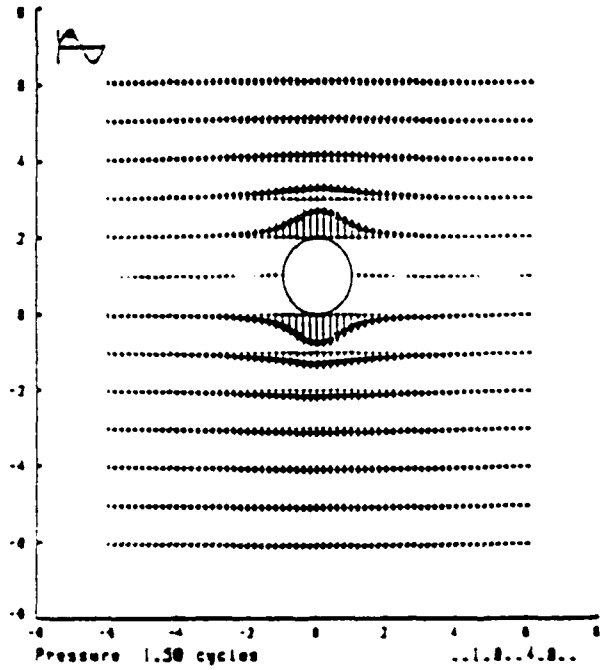

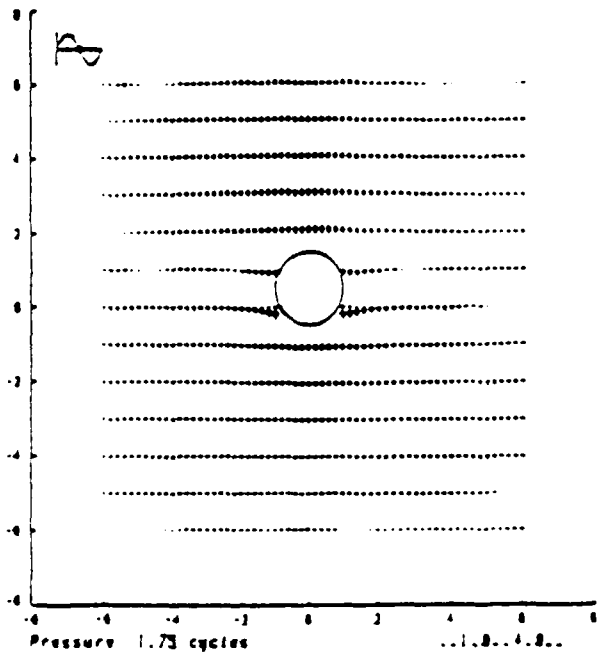

Figure 13(b) Pressure vectors for the Oscillating Cylinder (Ampl. = Rad.)

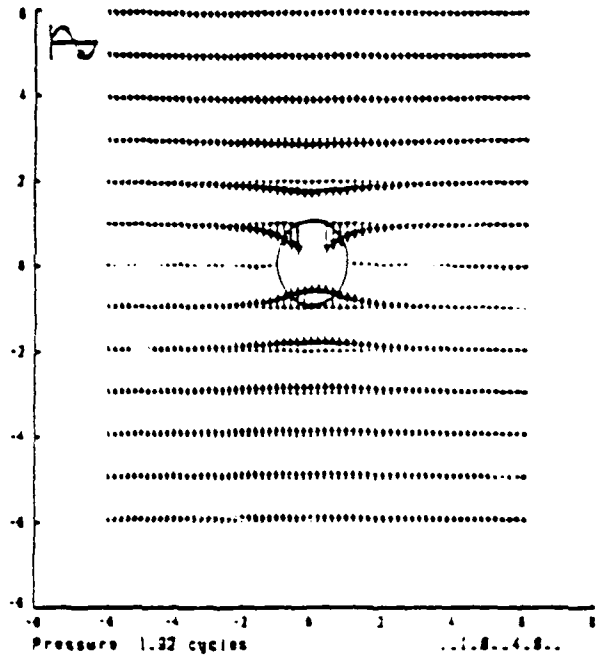

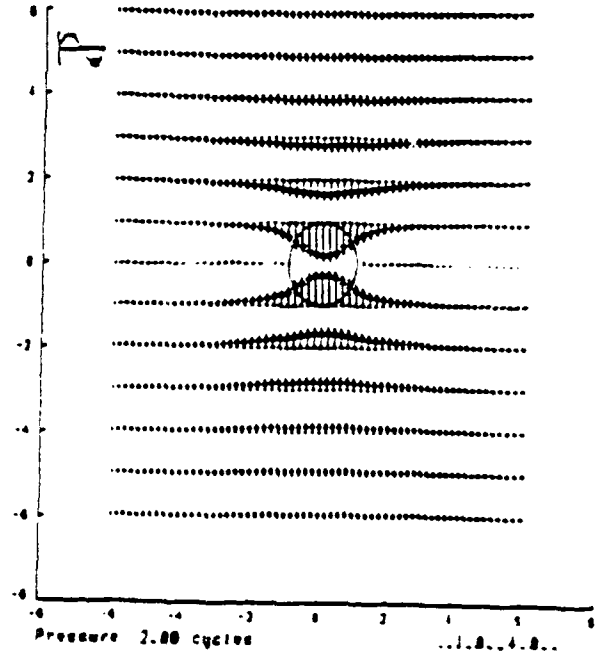

Figure 13(c) Pressure vectors for the Oscillating Cylinder (Ampl. = Rad.)

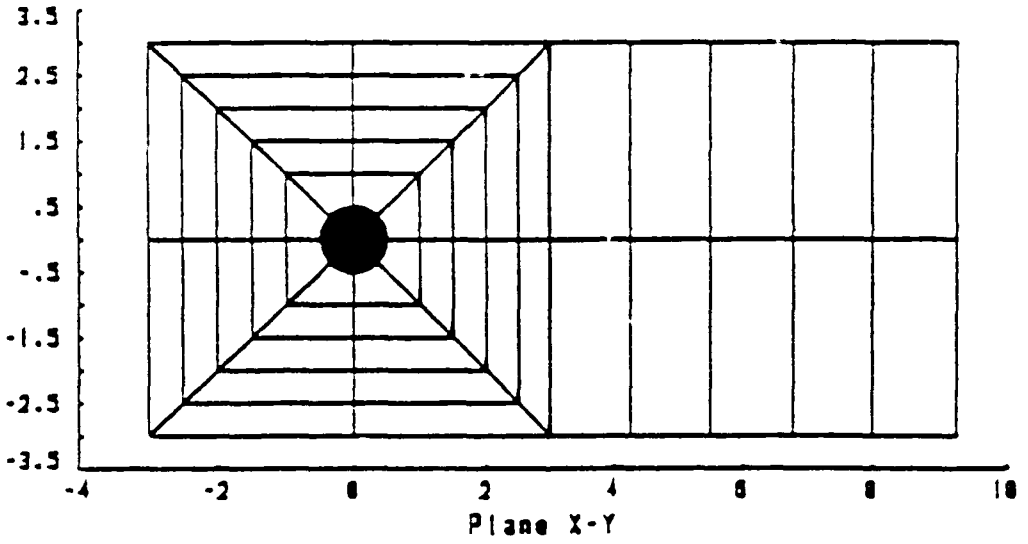

Figure 14 The Three-Dimensional Oscillating Cylinder Mesh

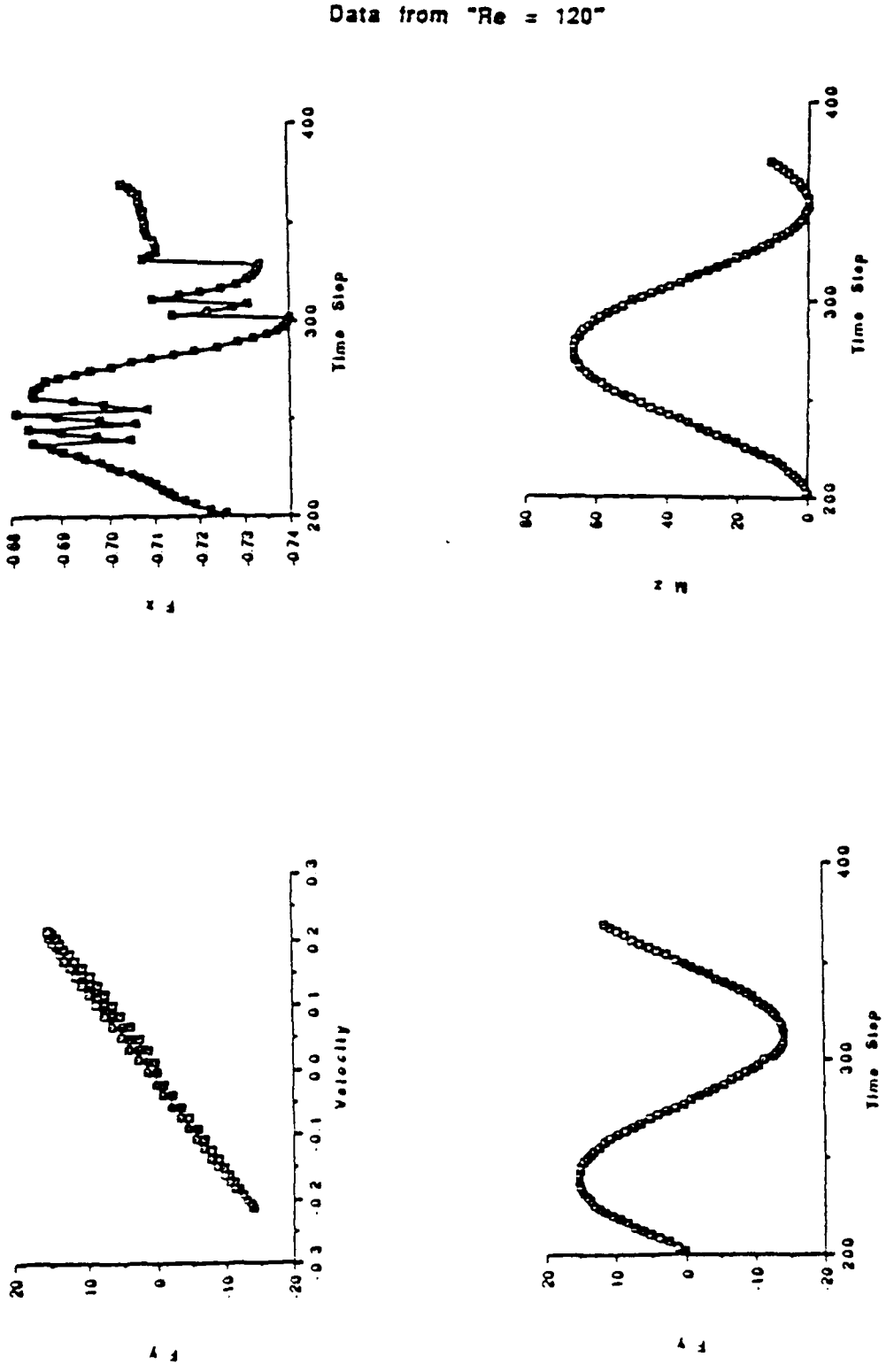

Figure 15 Forces and Moments on Cylinder at Re = 120

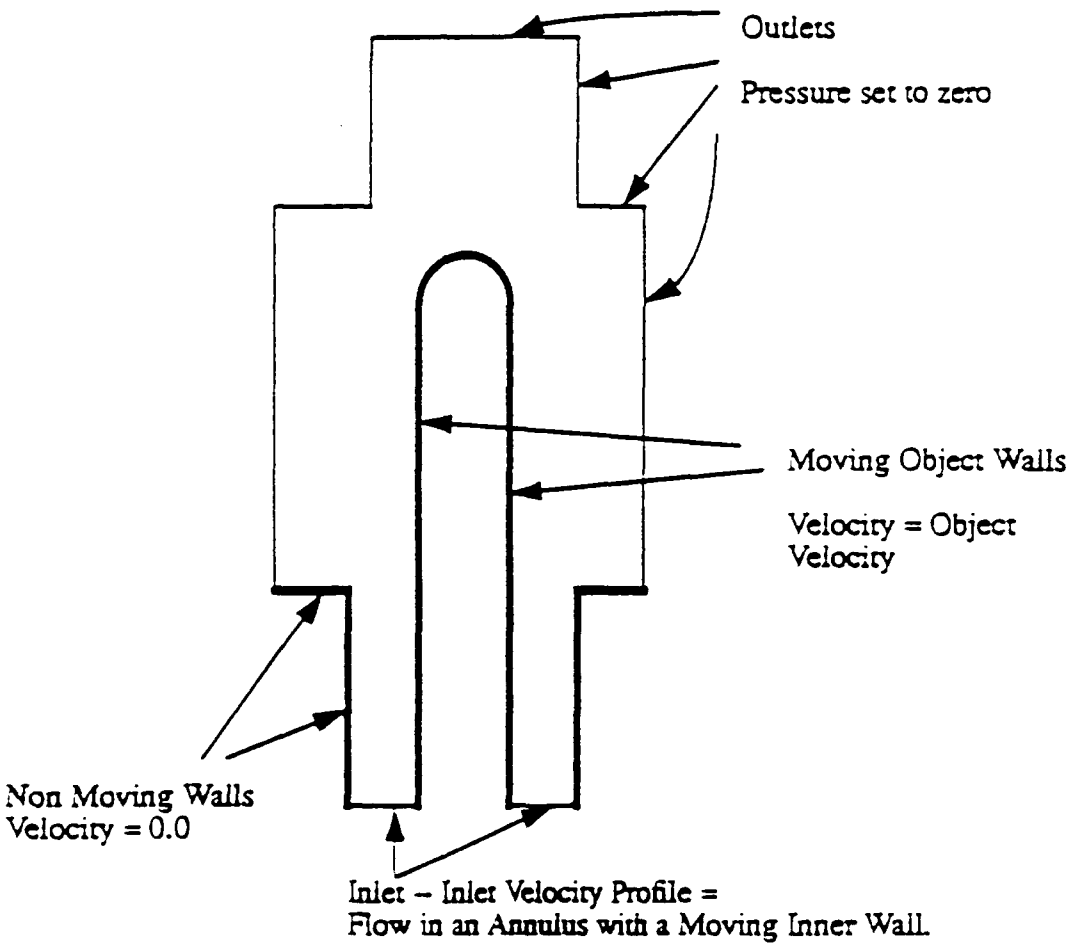

Figure 16 Schematic Drawing of the Separating Objects Mesh

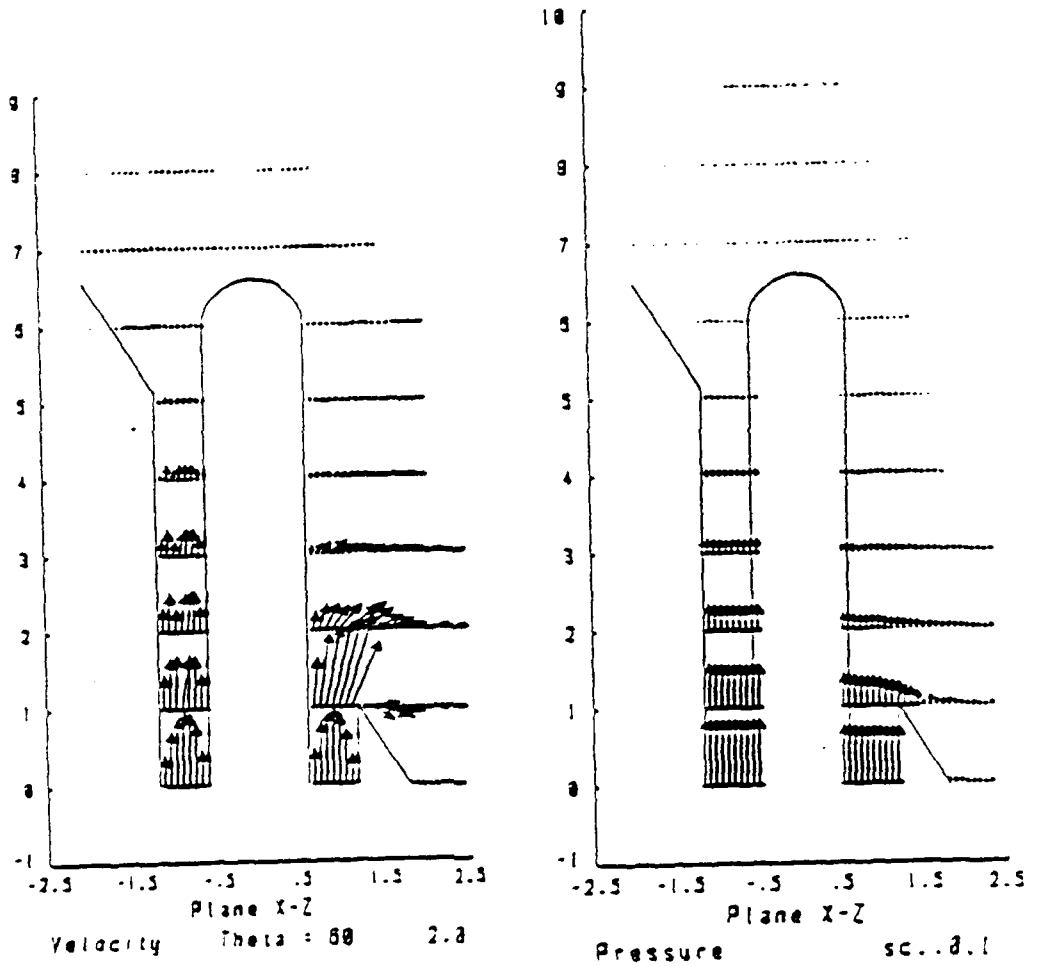

Figure 17 (a) Velocity and Pressure Plots of Theta = 60 Degrees

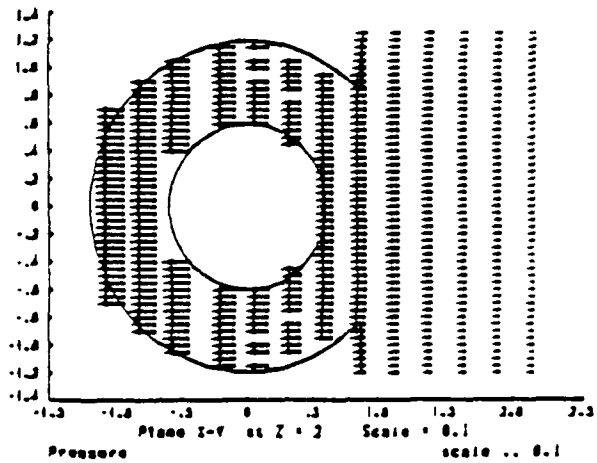

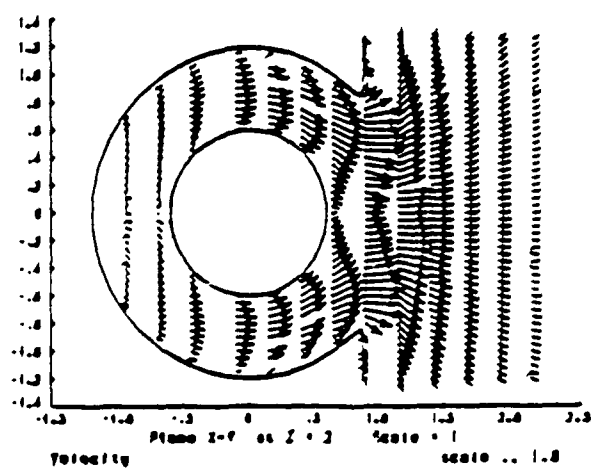

Figure 17 (b) Velocity and Pressure Plots of Theta = 60 Degrees

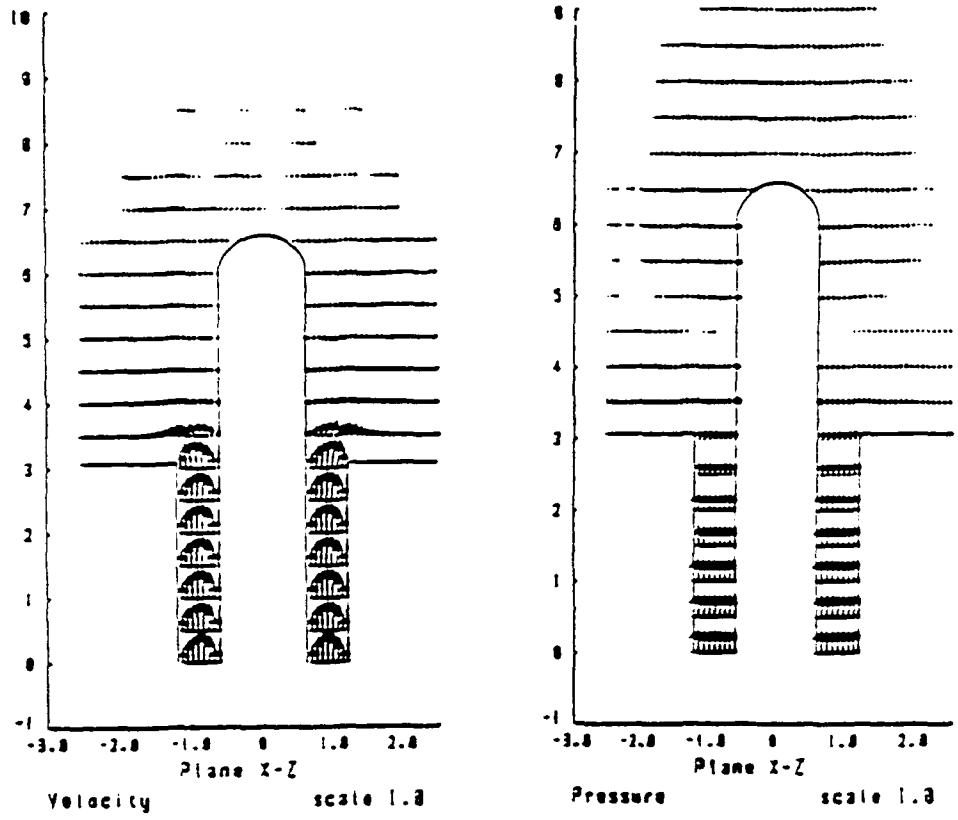

Figure 18 Velocity and Pressure Plots of Theta = 0 Degrees

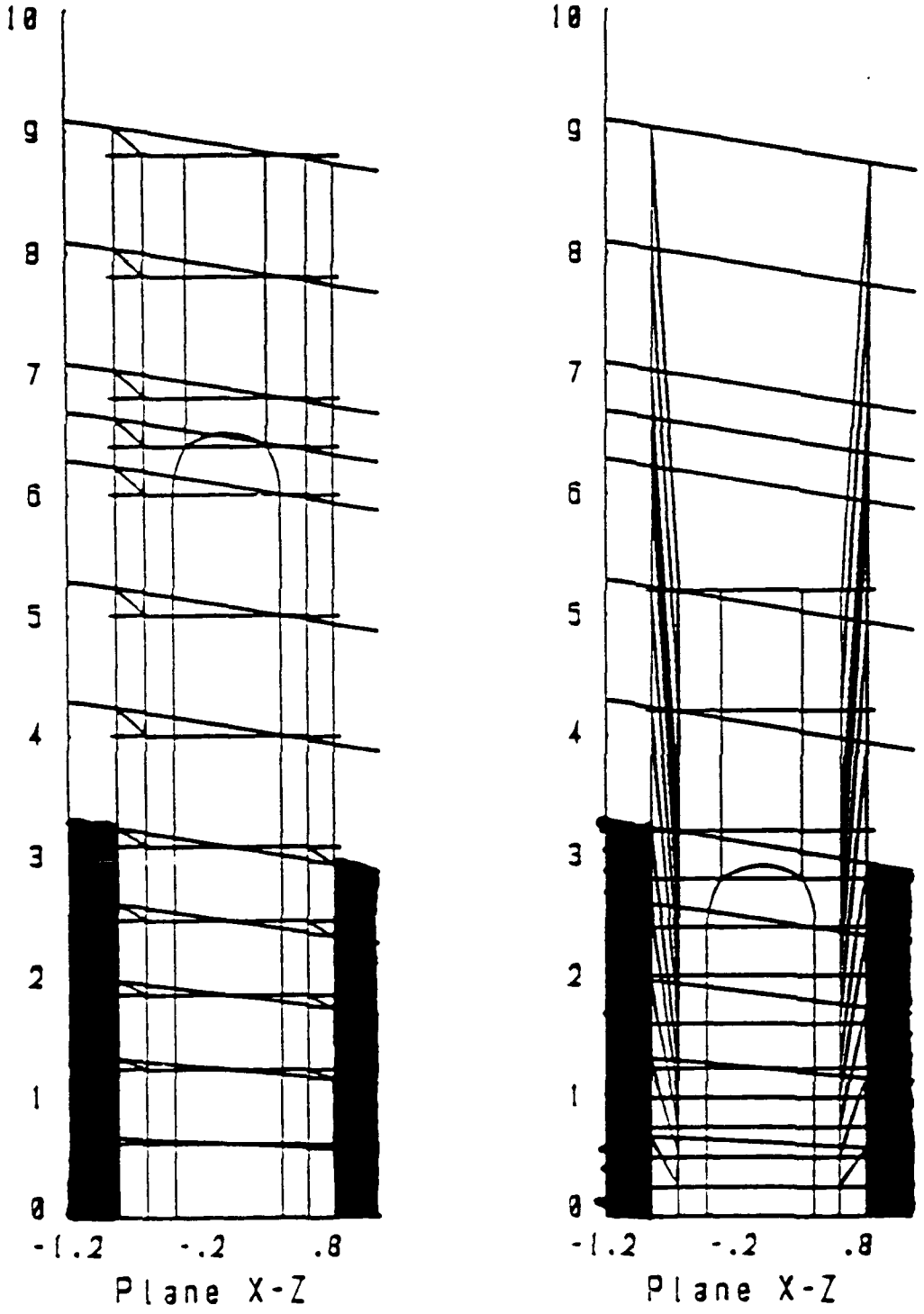

Figure 19 Example of Mesh Element Motion

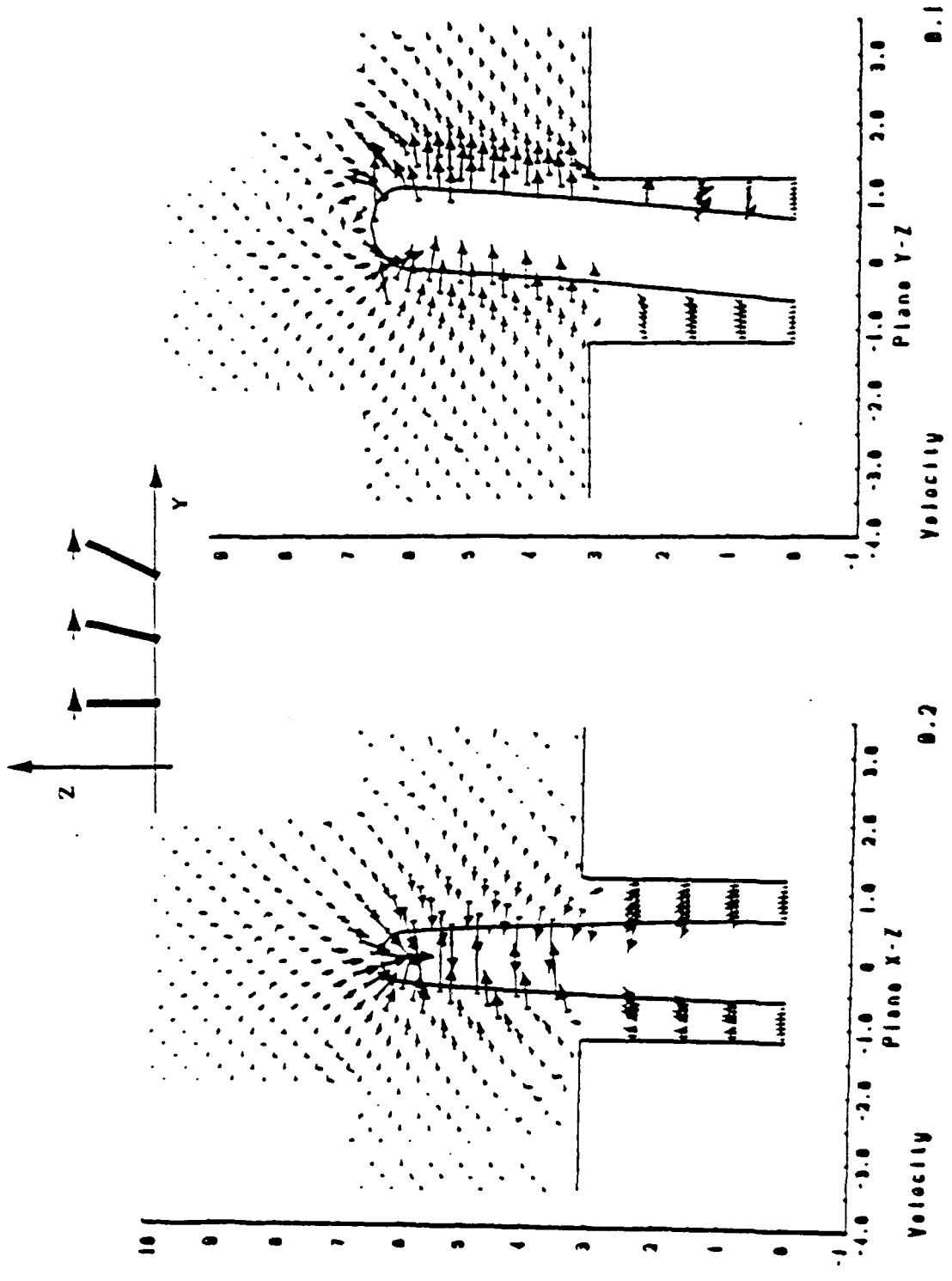

Figure 20 Velocity and Pressure Plots of Object Moving in Y Direction

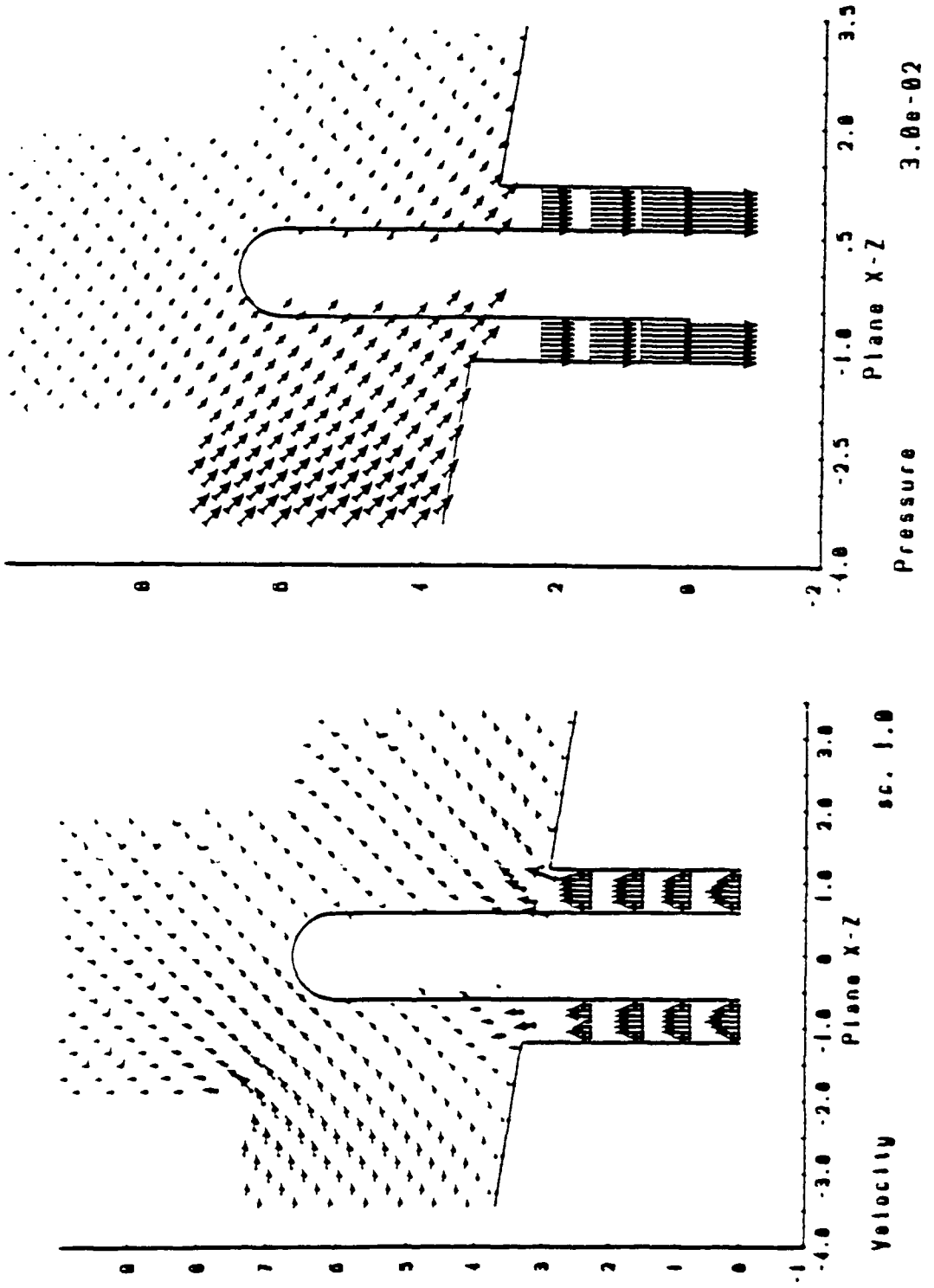

Figure 21. Velocity and Pressure Plots of Theta = 10 Degrees